

Charles University in Prague  
Faculty of Mathematics and Physics

## **DIPLOMA THESIS**



**Jan Fikáček**

### **The development of magnetic behavior in the $\text{PrNi}_{1-x}\text{Cu}_x\text{Al}$ compounds**

Department of Condensed Matter Physics

Supervisor: Doc. Mgr. Pavel Javorský, Dr.

Study brunch: Physics of Condensed Matter and Materials

2010

## Acknowledgments

To doc. Pavel Javorský, the supervisor of my diploma thesis, for many of his beneficial advices and very helpful assistance throughout the whole period of my working on this thesis.

To RNDr. Jiří Prchal for performing of the powder neutron diffraction experiment in ILL in Grenoble.

To Ing. Eva Šantavá, for her support during measurements on PPMS and MPMS instruments.

To Mgr. Klára Uhlířová and Mgr. Jiří Kaštil for their help during the preparation of my samples.

To Mgr. Jiří Pospíšil for his assistance during the preparation of samples on microprobe analysis and for his guidance during this measurement.

Prohlašuji, že jsem svou diplomovou práci napsal samostatně a výhradně s použitím citovaných pramenů. Souhlasím se zapůjčováním práce.

V Praze dne 20. 4. 2010

Jan Fikáček

# Contents

<b>1. Introduction</b> . . . . .	<b>5</b>
<b>2. Theory</b> . . . . .	<b>6</b>
2.1. Rare earths . . . . .	<b>6</b>
2.1.1. Magnetic interactions . . . . .	<b>7</b>
2.1.2. Crystal field effects . . . . .	<b>8</b>
2.1.3. Paramagnetic properties. . . . .	<b>9</b>
2.1.4. Spin glass state . . . . .	<b>9</b>
2.2. Theory of experimental methods . . . . .	<b>11</b>
2.2.1. X-ray diffraction . . . . .	<b>11</b>
2.2.2. Neutron diffraction. . . . .	<b>12</b>
2.2.3. Heat capacity. . . . .	<b>13</b>
<b>3. Previous results.</b> . . . . .	<b>15</b>
3.1. RTX compounds . . . . .	<b>15</b>
3.2. RCuAl, RNiAl . . . . .	<b>16</b>
3.3. PrCuAl, PrNiAl. . . . .	<b>16</b>
3.4. RNi <sub>1-x</sub> Cu <sub>x</sub> Al compounds. . . . .	<b>18</b>
<b>4. Experimental methods.</b> . . . . .	<b>20</b>
4.1. Sample preparation . . . . .	<b>20</b>
4.2. Powder X-ray diffraction . . . . .	<b>20</b>
4.3. Microprobe analysis . . . . .	<b>21</b>
4.4. Neutron diffraction . . . . .	<b>21</b>
4.5. Specific heat measurements . . . . .	<b>21</b>
4.6. Measurements of magnetization . . . . .	<b>22</b>
4.6.1. DC magnetization measurements . . . . .	<b>22</b>
4.6.2. Measurements of AC susceptibility . . . . .	<b>22</b>
<b>5. Results and discussion.</b> . . . . .	<b>23</b>
5.1. Crystal structure . . . . .	<b>23</b>
5.1.1. X-ray diffraction . . . . .	<b>23</b>
5.1.2. Microprobe analysis . . . . .	<b>25</b>
5.2. Paramagnetic region . . . . .	<b>28</b>
5.3. Magnetization measurements . . . . .	<b>31</b>
5.3.1. DC susceptibility . . . . .	<b>31</b>
5.3.2. AC susceptibility . . . . .	<b>36</b>
5.4. Heat capacity measurements . . . . .	<b>42</b>
5.5. Powder neutron diffraction . . . . .	<b>47</b>
<b>6. Conclusions.</b> . . . . .	<b>48</b>

Název práce: Vývoj magnetického chování ve sloučeninách  $\text{PrNi}_{1-x}\text{Cu}_x\text{Al}$

Autor: Bc. Jan Fikáček

Katedra: Katedra fyziky kondenzovaných látek

Vedoucí diplomové práce: Doc. Mgr. Pavel Javorský, Dr.

e-mail vedoucího: javor@mag.mff.cuni.cz

Abstrakt: V předložené práci jsme se zabývali studiem magnetických vlastností substituované série  $\text{PrNi}_{1-x}\text{Cu}_x\text{Al}$ . V dříve studovaných systémech se stejnou substitucí, ale jinou vzácnou zeminou, docházelo k velmi zajímavým magnetickým vlastnostem, např. vymizení dlouhodosahového uspořádání v určitém intervalu koncentrace mědi. Námi připravené polykrystalové vzorky  $\text{PrNi}_{1-x}\text{Cu}_x\text{Al}$  ( $x = 0.1 - 0.9$ , devět různých stechiometrií) byly měřeny pomocí rentgenové difrakce, měrného tepla, magnetizace a střídavé susceptibility. Na vzorku  $\text{PrNi}_{0.2}\text{Cu}_{0.8}\text{Al}$  byla navíc změřena prášková neutronová difrakce v ILL (Institut Laue Langevin) v Grenoble. Výsledky měření na těchto sloučeninách ukazují na přítomnost dlouhodosahového antiferomagnetického uspořádání pro sloučeniny ( $x = 0.1 - 0.4$ ) pod teplotami uspořádání v intervalu 3.4 – 5 K. Měření střídavé susceptibility a neutronové difrakce odhalila vymizení dlouhodosahového uspořádání pro zbytek série. V těchto sloučeninách dochází ke vzniku stavu spinového skla pod teplotami 3.4 – 4.5 K.

Klíčová slova: vymizení dlouhodosahového uspořádání, spinová skla, střídavá susceptibilita.

Title: The development of magnetic behavior in the  $\text{PrNi}_{1-x}\text{Cu}_x\text{Al}$  compounds

Author: Bc. Jan Fikáček

Department: Department of Condensed Matter Physics

Supervisor: Doc. Mgr. Pavel Javorský, Dr.

Supervisor's e-mail address: javor@mag.mff.cuni.cz

Abstract: In the present work we studied magnetic properties of the substituted  $\text{PrNi}_{1-x}\text{Cu}_x\text{Al}$  series. A very interesting behavior had been reported in the previously studied systems with the same substitution, but with different rare earths contained, e.g. loss of long range order for certain concentrations of copper. We prepared polycrystalline samples of the  $\text{PrNi}_{1-x}\text{Cu}_x\text{Al}$  ( $x = 0.1 - 0.9$ , 9 different stoichiometries) and measured them using X-ray diffraction, specific heat, magnetization and AC susceptibility. Additionally, powder neutron diffraction measurement on  $\text{PrNi}_{0.2}\text{Cu}_{0.8}\text{Al}$  sample was performed in ILL (Institut Laue Langevin) in Grenoble. Results of measurements on these compounds show on the presence of a long order in case of compounds with  $x = 0.1 - 0.4$  below the ordering temperatures in the range of 3.4 – 5 K. Measurements of AC susceptibility and neutron diffraction revealed the loss of long range order in the rest of the series. In these compounds, the development of a spin glass state occurs below the temperatures between 3.4 and 4.5 K.

Keywords: loss of long range order, spin glasses, AC susceptibility.

## 1. Introduction

The ternary intermetallic RTX compounds (R = rare earth, T = transition metal, X = p-metal) crystallizing in the hexagonal ZrNiAl-type structure form a rather large group. The studies focused on their magnetic properties often show very complex and surprising behavior. The underlying microscopic mechanisms have not been satisfactory clarified up to now. Very interesting seems to be the loss of the long-range magnetic order for certain Cu concentrations in  $\text{RNi}_{1-x}\text{Cu}_x\text{Al}$  with R = Tb, Dy, Er and Nd. This feature seemed to be independent on the rare-earth ion. The neutron diffraction study performed on PrCuAl gave qualitatively different results from other RCuAl. Additionally, very recently performed measurements on the Nd-based  $\text{RNi}_{1-x}\text{Cu}_x\text{Al}$  series revealed slightly different properties related to the loss of the long-range magnetic order. The ordering temperatures in PrCuAl and PrNiAl are exceptionally high. The Pr, as another member of light rare earth atoms, is highly expected to form the series of compounds which might represent a case with different magnetic interactions than the heavy rare earth based  $\text{RNi}_{1-x}\text{Cu}_x\text{Al}$  compounds. It is therefore worth to investigate the  $\text{PrNi}_{1-x}\text{Cu}_x\text{Al}$  system and compare with the other  $\text{RNi}_{1-x}\text{Cu}_x\text{Al}$  series.

In this work we present results on our polycrystalline samples with different parameter  $x$  chosen to reasonably describe the whole  $\text{PrNi}_{1-x}\text{Cu}_x\text{Al}$  series. The samples were measured by X-Ray diffraction and Microprobe analysis in order to obtain information about the crystal structure. Magnetic properties were investigated by measurements of magnetization in homogenous (DC susceptibility) and time dependent magnetic fields (AC susceptibility), by specific heat and last but not least by powder neutron diffraction on one selected sample.

This thesis has the following organization. We start with description of theory needed for basic understanding of properties owned by rare earth compounds and experimental methods used in this work in Chapter 2. Theory. It is followed by summary of previous results published before the finishing of this thesis on compounds related to our series in Chapter 3. Previous results. Next Chapter, 4. Experimental methods, contains brief description of measurement procedures performed for collecting the experimental data. These data are included and discussed in Chapter 5. Results and discussion. Our main findings are additionally discussed in 6. Conclusions.

## 2. Theory

### 2.1. Rare earths

The group in the periodic table of elements located between lanthanum (La<sup>57</sup>) and lutetium (Lu<sup>71</sup>) is called lanthanides. Together with scandium (Sc<sup>21</sup>) and yttrium (Y<sup>39</sup>), lanthanides form the rare earths. They can be additionally divided on light rare earths (from La to Eu) and heavy rare earths (from Gd to Lu).

The electronic configuration of rare earths can be expressed by

$$[\text{Xe}] 6s^2 5d^1 4f^N,$$

4f-shell electrons, the only one responsible for rare earths magnetic moment, are well shielded in a solid by the more delocalized 6s and 5d-shells. Thus any magnetic order in rare earth compounds (with no other magnetic ions) cannot take place directly by the interaction of magnetic ions but through some more complex mechanism. That is discussed in the following chapter.

Energy levels in an atom are split into so called terms characterized by values of the total orbital momentum  $L$  and the total spin momentum  $S$ . Since  $L_z$  can take values in the range  $-L, \dots, L$  and  $S_z$  values in the range  $-S, \dots, S$ , electrons in an atom could organize in  $(2L+1)(2S+1)$  ways. For the determination of the rare earths ground state, there is an appropriate to use Russell-Saunders approximation (Hund's rules [22]). The basic assumption of this approximation is that the main interaction, affecting positions of electrons in an unfilled shell, is Coulomb repulsion. The next most important factor is the spin-orbit interaction which is introduced as a small perturbation.  $L$  and  $S$  values are determined in a way which obeys first two empiric Hund's rules. The total angular momentum  $J$ , which connects  $S$  and  $L$ , takes the values from  $|L - S|$  to  $L+S$ . Adding of the spin-orbit interaction causes that  $J$  is counted for less than half full electron shell (Pr<sup>3+</sup>) by  $J = |L - S|$  (third Hund's rule). The energy levels of an atom will be then  $(2J+1)$ -fold degenerate. According to this result we can evaluate effective magnetic moment of Pr<sup>3+</sup> using

$$\mu_{\text{eff}} = g_J \cdot \mu_B \sqrt{J \cdot (J+1)}, \quad (1)$$

where  $\mu_B$  is Bohr magneton and  $g_J$  is Landé g-factor reflecting projection of the total spin momentum  $S$  and the total orbital momentum  $L$  onto the direction of the total angular

momentum  $J$

$$g_J = \frac{3J.(J+1) + S.(S+1) - L.(L+1)}{2J.(J+1)}. \quad (2)$$

### 2.1.1. Magnetic interactions

The occurrence of a magnetic ordering in materials is generally determined by some kind of magnetic interactions. They can be divided into two groups – direct and indirect ones.

Magnetic dipolar interaction is the first type of direct interaction. It is caused by dipolar interaction between two magnetic moments. This interaction is very weak as the strength is of the order of 1 K and can be very often neglected.

The second type of direct interaction is direct exchange interaction. Direct because it is arising between two neighboring magnetic ions and exchange because the interaction is boosted by reducing of Coulomb interaction energy through the delocalizing of electrons to neighboring atoms. Direct exchange interaction is mainly limited by the distance between neighboring magnetic orbitals. In case of 4f orbitals it can be also neglected.

Indirect exchange interactions are more commonly considered as responsible for a long range ordering of the most of magnetic materials. Especially in compounds with well localized 4f orbitals of rare earth atoms. Indirect exchange interactions between magnetic ions are mediated via neighboring nonmagnetic ions or by conduction electrons. The first type is also known as superexchange and can be found for example in some oxides and fluorides. The second mechanism is very often responsible for magnetic ordering in metals, including RTX compounds, and is known as the RKKY interaction [7].

The RKKY interaction originates in spin-polarization of conduction electrons by magnetic ions. Those electrons couple to neighboring magnetic ions. For the RKKY interaction, like for other exchange interactions, one can write Heisenberg Hamiltonian:

$$H_{RKKY} = -\sum \mathcal{J}(r_i - r_j).J_i.J_j, \quad (3)$$

where  $J_i$  and  $J_j$  are total angular momenta of neighboring magnetic ions and  $\mathcal{J}(r_i - r_j)$  takes the following form:

$$J(r) = \frac{(r \cdot \cos r - \sin r)}{r^4}, \quad (4)$$

where  $r$  is the distance between the two interacting ions. The exchange constant  $J$  shows that the effect of RKKY is oscillating with distance between magnetic ions. Thus it can favor both ferromagnetic and antiferromagnetic order.

In RTX compounds two possible ways to realize the interaction among magnetic ions are discussed in the literature. Beside the RKKY interaction, an interaction mediated by d-electrons was described by Campbell [17]. It is expected to rise due to the interaction of rare earth 5d-electrons and rare earth 4f-electrons which induces a local d-moment. The 5d-electrons of a rare earth ion, which are more delocalized than the 4f ones, can subsequently directly interact with 5d-electrons of neighboring rare earth ions. Additionally, in compounds with a transition metal, we can consequently expect another strengthening due to interaction of the 5d-electrons with d-electrons of the transition metal.

### 2.1.2. Crystal field effects

If a rare earth atom is placed in a crystal, its 4f electrons are influenced by other ions and electrons localized in its vicinity. All those elements form the electric field which is called crystal field. Crystal field can partially or fully remove the degeneracy of the ground state multiplet. As mentioned above, 6s and 5d shells shield the 4f-shell and therefore also weaken the crystal field acting on them.

Energy levels of the rare earth ion in a crystal field can be determined by calculation of the crystal field Hamiltonian matrix elements. The crystal field Hamiltonian can be written as

$$\hat{H}_{CF} = \sum_{n,m} B_n^m \hat{O}_n^m, \quad (5)$$

where  $B_n^m$  and  $\hat{O}_n^m$  are the crystal field parameters and operators, respectively [21].

### 2.1.3. Paramagnetic properties

In the paramagnetic state the magnetic moments of atoms are randomly oriented due to overbearing thermal fluctuations. Therefore the net magnetization in a paramagnetic state is zero. Application of an external magnetic field causes partial orientation of moments in the field direction resulting in a raise of the volume magnetization. One can quantify this effect using magnetic susceptibility  $\chi$

$$\chi = \frac{M}{H} = \frac{N_A \mu_0 \mu_B^2 \mu_{eff}^2}{3k_B(T - \theta_p)} + \chi_0, \quad (6)$$

where  $N_A$  is Avogadro's constant,  $\mu_0$  is vacuum permeability,  $k_B$  is Boltzmann's constant and  $\theta_p$  is paramagnetic Curie temperature. The last term  $\chi_0$  is highly suitable to be added into the equation if one wants to describe the effect of Van Vleck paramagnetism and influence by the anisotropy, when the  $\theta_p$  vary significantly along different axes.  $\chi_0$  consequently corrects the certain curvature raising mainly due to these two phenomena.

### 2.1.4. Spin glass state

The principle of a spin glass state is the existence of a freezing temperature below which all the magnetic moments in a compound stay frozen in a random orientation. Only short-range correlations may be present.

Several mechanisms can be responsible for the development of a spin glass state. One of them is a geometrical frustration of magnetic moments. That is a state when magnetic moments in certain positions of a crystal lattice have more equivalent possibilities for their orientation which leads to inability of the system to find a single ground state. Together with combination of antiferromagnetic (also with some ferromagnetic) interactions between different sets of moments, the spin glass state can be highly preferred as a magnetic structure for a given material. RKKY interaction with its oscillating character is very likely favorable for the evoking of a moments frustration.

There are a few types of spin glass states. For us the most important are canonical spin glass and cluster glass systems [23]. The latter one is characterized by the existence of areas in a volume (clusters) which can magnetically interact among each other.

Measurement of AC susceptibility is one of most suitable tools for inspecting spin glass

properties. Characteristic relaxation time  $\tau$  of a spin glass system is several orders higher than it is in case of a long range ordered material. Therefore relatively lower frequencies ( $f = 2\pi/\tau$ ) of an oscillating magnetic field are enough to cause a measurable shifting of a freezing temperature. On the other hand, the frequencies needed to produce shifting of a transition temperature in a long range ordered material are of the order of  $10^6$  Hz. So the AC susceptibility can truly distinguish whether a material is long range ordered or not.

To obtain physical values characterizing spin glass state one can use the Néel-Arrhenius law [24, 25]:

$$f = f_0 \cdot \exp\left(-\frac{E_A}{k_B \cdot T_f}\right), \quad (7)$$

where  $E_A$  is the activation energy of the freezing process and  $T_f$  is the freezing temperature corresponding to the frequency  $f$  of the applied oscillating magnetic field. The Néel-Arrhenius law is more suitable for a non interacting superparamagnetic system. In case of spin glass clusters, the Vogel-Fulcher law [26] gives more physical results of  $E_A$  and  $f_0$ :

$$f = f_0 \cdot \exp\left(-\frac{E_A}{k_B \cdot (T_f - T_{VF})}\right). \quad (8)$$

Vogel-Fulcher law is a modified Néel-Arrhenius law. Hence, additionally, it establishes  $T_{VF}$ . Although it lacks any exact physical meaning,  $T_{VF}$  relates to the strength of interaction among spin glass clusters. Higher the temperature is, higher interaction of clusters can be expected.

Another useful criterion, which helps to decide whether treat the system using the Néel-Arrhenius or the Vogel-Fulcher law, is the parameter of  $\delta T_f$  defined as:

$$\delta T_f = \frac{\Delta T_f}{T_f \cdot \Delta \ln f}. \quad (9)$$

Comparing an obtained value with those in similar systems one can choose which one of the laws should be used.

## 2.2. Theory of experimental methods

In the following chapter the basic theoretical background of the experimental methods used during experiments for this work is mentioned.

### 2.2.1. X-ray diffraction

X-ray diffraction is a powerful tool to obtain information about crystallographic structure of the given compound. The total cross section of Thomson's scattering on free ion is inverse proportional to particle weight, therefore X-rays interact only with electron shells of atoms. X-ray beam is diffracted by crystallographic planes into different directions according to the Bragg's law:

$$2d_{hkl} \cdot \sin \theta_{hkl} = \lambda, \quad (10)$$

where  $d_{hkl}$  is the inter-planar distance of diffracting planes,  $\theta_{hkl}$  is diffraction angle set by the incident beam and normal of the diffracting (hkl) plane and  $\lambda$  is the wavelength of the incident X-ray beam.

The diffracted intensity is proportional to the square of the structure factor

$$I \approx |F_{hkl}|^2, \quad (11)$$

which is in case of X-ray diffraction given by

$$F_{hkl} = \sum_j f_j(\mathbf{q}) \cdot e^{-i\mathbf{q} \cdot \mathbf{r}_j} e^{-W_j}. \quad (12)$$

The summation is taken over the unit cell. The atomic scattering factor  $f_j(\mathbf{q})$  is a function of scattering vector  $\mathbf{q}$  and for a selected atom it is given by the Fourier transformation of its charge density. The last term in the equation is the correction on thermal vibrations, called Debye-Waller factor.

Powder X-ray diffraction was measured in this work. The biggest advantage of this method is simplicity in preparation of samples and low measurement time. This kind of measurement gives values of lattice parameters and can roughly show amount of impurity

phases in the given sample.

### 2.2.2. Neutron diffraction

The main difference between neutron and X-ray diffraction is that neutrons interact with atomic nuclei. The Bragg's equation (10) remains valid, of course. The measured intensity of diffraction is given by square of the atomic structure factor  $F_{hkl}$ , which can be expressed by:

$$F_{hkl} = \sum_j b_j \cdot e^{i \cdot q \cdot r_j} \cdot e^{-W_j} , \quad (13)$$

$b_j$  are coherent scattering lengths, which is a characteristic value of the given isotope and are tabulated e.g. in [28].

Additionally, in case of magnetic ordered material, neutrons also coherently diffract on magnetic moment of atom via their spin. If the studied compound develops magnetic ordering, which can be described by certain propagation vector(s)  $\mathbf{k}$ , the diffracted magnetic intensities are given at reciprocal space by:

$$\mathbf{q} = \mathbf{h} \pm \mathbf{k} . \quad (14)$$

The magnetic structure factor can be expressed in the following formula:

$$F_m(\mathbf{q}) = \sum_j f_j(\mathbf{q}) \cdot \boldsymbol{\mu}^k \cdot e^{i \cdot \mathbf{q} \cdot \mathbf{r}_j} \cdot e^{-W_j} , \quad (15)$$

where  $f_i(\mathbf{q})$  is the magnetic form factor (exact expression for individual can be found e.g. in [29]).  $\boldsymbol{\mu}^k$  is the projection of the magnetic moment into the plane perpendicular to the diffraction vector  $\mathbf{q}$  which is given by difference between the incident and the scattered wave vector. The sum is taken over all magnetic moments within the unit cell.

Resulting intensity, in case of unpolarized neutrons, is then given by the sum of squares of the structure factor and of the magnetic structure factor.

### 2.2.3. Heat capacity

There are three main contributions to the specific heat of rare earth compounds:

$$C = C_{el} + C_{phon} + C_{mag}, \quad (16)$$

$C_{el}$  is electron heat capacity, which is proportional to the temperature, according to

$$C_{el} = \frac{1}{3} \pi^2 n(E_F) k_B^2 T = \gamma T, \quad (17)$$

$n(E_F)$  is the density of states at the Fermi level [27].  $\theta_{Ei}$  is characteristic Einstein temperature.  $C_{phon}$  is phonon contribution given by:

$$C_{phon} = 9k_B N_A (T/\theta_D)^3 \int_0^{\theta_D/T} \frac{x^4 e^x}{(e^x - 1)^2} dx + k_B N_A \sum_{i=1}^6 (\theta_{Ei}/T)^2 \frac{e^{\theta_{Ei}/T}}{(e^{\theta_{Ei}/T} - 1)^2}. \quad (18)$$

$\theta_D$  is characteristic Debye temperature. This formula reduces to a simple  $\sim T^3$  dependence at low temperatures ( $T < \theta_D/20$ ) [27]. These two contributions can be both often subtracted through the use of specific heat of a similar nonmagnetic compound.

After the subtraction of electron and phonon contributions, magnetic specific heat  $C_{mag}$  remains. In the paramagnetic state it is also called Schottky contribution. Schottky specific heat reflects changes of the population of energy levels

$$C_{Sch} = \frac{-\partial^2 (k_B T \ln Z)}{\partial T^2}, \quad (19)$$

where  $Z$  is the partition function

$$Z = \sum_i e^{-E_i/k_B T}. \quad (20)$$

The electron energy levels  $E_i$  (crystal-field levels) can be thus determined by analyzing of this specific heat contribution. From the magnetic specific heat we can also calculate the amount of connected entropy

$$S(T^*) = \int_0^{T^*} \frac{C_{mag}}{T} dT . \quad (21)$$

As the ground state multiplet of the  $R^{3+}$  ion is split due to the crystal field into  $(2J+1)$  energy levels, the magnetic entropy should reach

$$S = R \cdot \ln(2J+1). \quad (22)$$

### 3. Previous results

#### 3.1. RTX compounds

The RTX compounds consist of one rare earth atom (R), one atom of transition metal (T) and one atom with partially unfilled p-shell – p-metal (P). Most of them (for T = Cu, Ni, Pd) crystallize in the hexagonal ZrNiAl structure type, which has the space group P-62m. The structure is characterized by existence of two types of basal planes. In the first one there are only transition metal atoms at positions  $(1/3, 2/3, 0)$ ,  $(2/3, 1/3, 0)$  and atoms of p-metal at positions  $(x, 0, 0)$ ,  $(0, x, 0)$  and  $(-x, -x, 0)$ , in the second type the transition metal atoms are at positions  $(0, 0, 1/2)$  and rare earth atoms at positions  $(y, 0, 1/2)$ ,  $(0, y, 1/2)$  and  $(-y, -y, 1/2)$ . These two layers periodically alternate in direction of the z-axis, see Fig. 3.1. and Fig. 3.2.

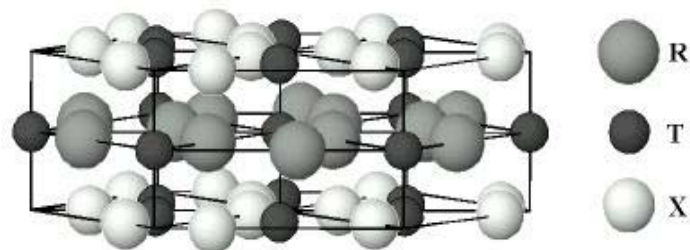


Fig. 3.1.: The RTX structure, taken from [38].

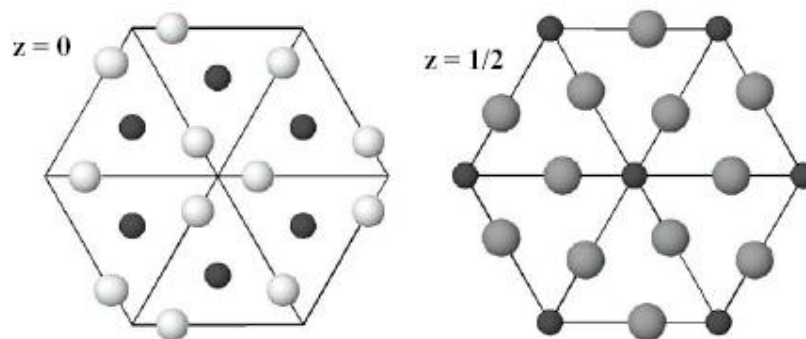


Fig. 3.2.: View on the basal planes of the RTX structure, taken from [38].

RTX compounds show very interesting behavior due to well localized 4f-shells (lanthanides) of rare earth atoms. These magnetic ions usually do not have any different possibility of interaction among each other than by the RKKY bond (Ruderman-Kittel-Kasuya-Yosida), which is mediated by conduction electrons [7]. The RKKY interaction is, among others, depending on the distance between neighboring magnetic ions and the amount of conduction electrons. Very interesting changes in magnetic behavior are observed when substituting the T or X elements, which is mostly limited by conservation of the crystal structure.

### 3.2. RCuAl, RNiAl

There will be mentioned some compounds, which have connection to our deal of study.

The first ones are RCuAl, which order ferromagnetically (for Gd - Er) and antiferromagnetically for Pr, Nd or Tm. The Néel temperatures of PrCuAl ( $T_N = 7.9$  K) and NdCuAl ( $T_N = 18$  K) are higher than De Gennes scale factor predicts, considering the ordering temperature in GdCuAl [2]. This is an indication that there could be a different type of magnetic interactions in compounds with light rare earth atoms (Pr and Nd).

The most of RNiAl compounds order antiferromagnetically or show a co-existence of antiferromagnetic and ferromagnetic components at the lowest temperatures. The usual propagation vector of magnetic structure is  $\mathbf{k} = (1/2, 0, q)$ , where  $q = 0.5$  for R = Tb, Dy, Ho, Er and  $q < 0.5$  for Pr and Nd [5]. In other words RNiAl, compounds also differ in magnetic structure in dependence if there is a light or a heavy rare earth atom in compound, as it is in case of RCuAl. NdNiAl and PrNiAl, the light rare earth ones, have incommensurate magnetic structures, whereas RNiAl compounds with heavy rare earths have commensurate structures. Frustrated moments exist in several compounds as a result of triangular arrangement of the R atoms. Further magnetic phase transition is characterized by magnetic moment components within the basal plane (DyNiAl, HoNiAl) [6].

Several compounds from this family undergoes a jump in lattice parameters, which is connected with so called banned value of  $c/a$  lattice parameters ratio. There were not discovered any coherence between the banned ratio and magnetic structure [1].

### 3.3. PrCuAl, PrNiAl

PrCuAl orders antiferromagnetically with the Néel temperature  $T_N = 7.9$  K. The magnetic structure of PrCuAl can be described by the propagation vector

$\mathbf{k} = (1/3, 1/3, 1/3)$  [3], see Fig. 3.3., which differs from the usual propagation vector  $\mathbf{k} = (1/2, 0, q)$  occurring in other RCuAl and RNiAl compounds. In PrCuAl there is no metamagnetic transition until magnetic field up to 6 T [4]. The ordering temperature is just moving to lower values with increasing magnetic field. The value of magnetic moment is  $2.9 \mu_B$ , which is close to the moment of the free ion  $\text{Pr}^{3+}$  of  $3.58 \mu_B$ .

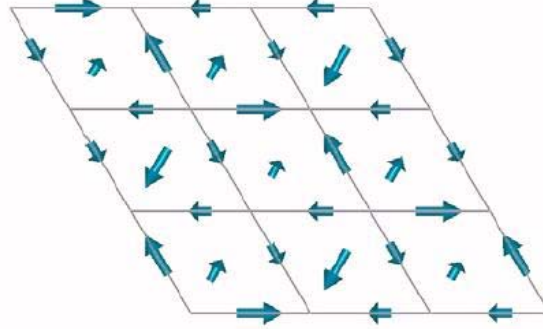


Fig. 3.3.: View on magnetic structure of PrCuAl in its basal plane. The structure can be described by the propagation vector  $(1/3, 1/3, 1/3)$ . The picture is taken from [30].

PrNiAl has an antiferromagnetic magnetic structure with ordering temperature  $T_N = 6.5$  K. The structure is, in contrast with PrCuAl, incommensurate with the propagation vector  $\mathbf{k} = (1/2, 0, 0.41)$ , see Fig. 3.4. A metamagnetic transition occurs with the magnetic field of 6 T when the temperature is 4.2 K. The value of magnetic moment is rising with increasing magnetic field, but it is not saturated until 35 T, when its value is  $2.0 \mu_B$  [8] which is far from the free ion  $\text{Pr}^{3+}$  value.

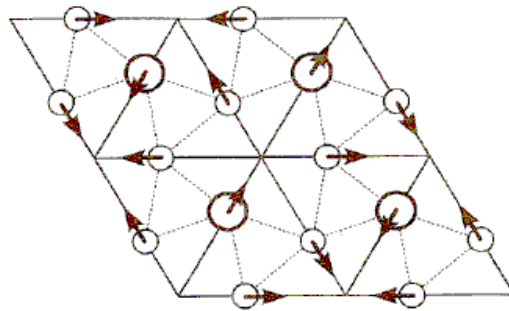


Fig. 3.4.: Magnetic structure in the basal plane of PrNiAl. The structure is characterized by the propagation vector  $(1/2, 0, 0.41)$ . In the direction which is perpendicular to the basal plane an incommensurate magnetic structure is formed. The picture is taken from [31].

### 3.4 RNi<sub>1-x</sub>Cu<sub>x</sub>Al compounds

Development of magnetic behavior was studied in several RNi<sub>1-x</sub>Cu<sub>x</sub>Al series. The first studied group was TbNi<sub>1-x</sub>Cu<sub>x</sub>Al [9]. Both TbCuAl and TbNiAl have the ZrNiAl crystal structure. TbNiAl orders antiferromagnetically below  $T_N = 47$  K, when one third of Tb magnetic moments is frustrated. Below the temperature of 23 K there is another magnetic phase transition, in which there is only a change of these frustrated moments. TbCuAl is, on the other hand, ferromagnetic below  $T_C = 51$  K. Substitution of Ni and Cu does not only change the lattice parameters, but also the type of magnetic structure, value of transition temperature and Curie-Weiss paramagnetic temperature. In the lowest amount of Cu concentration ( $x = 0.01 - 0.1$ ) both ferromagnetic and antiferromagnetic ordering is present at different parts of the material. With increasing part of Cu ( $x > 0.15$ ) the antiferromagnetic ordering changes into ferromagnetic one. By further increase of Cu ( $x = 0.6 - 0.8$ ) the long-range ordering vanishes and is replaced by short-range ordering. The RKKY bond in PrNiAl is mostly generated by 3-d electrons of Ni. By contrary, in case of TbCuAl, the bond between magnetic ions is mediated by s-electrons of Cu. The existence of the gap in long-range ordering is explained by that change of type of electrons mediating the bond between magnetic ions. Finally, for  $x > 0.8$  the ferromagnetic ordering appears again.

Another series which was studied by change of Ni-Cu stoichiometry is ErNi<sub>1-x</sub>Cu<sub>x</sub>Al. Pure ErNiAl is antiferromagnetic below the temperature  $T_N = 6.2$  K with propagation vector  $\mathbf{k} = (1/2, 0, 1/2)$ , the moments are within the basal plane. In contrast, ErCuAl is ferromagnetic below temperature  $T_C = 6.8$  K with moments along the z-axis [10]. Above mentioned discontinuity in lattice parameters appears in nearly equal amount of Cu and Ni in ErNi<sub>1-x</sub>Cu<sub>x</sub>Al ( $x = 0.5 - 0.6$ ). With increasing part of Cu in ErNi<sub>1-x</sub>Cu<sub>x</sub>Al (from  $x = 0.2$  up to  $x = 0.4$ ) incommensurate structure appears and moments in the basal plane are gradually weakened. ErNi<sub>0.5</sub>Cu<sub>0.5</sub>Al is simply ferromagnetic with moments completely aligned along the z-axis. A short-range ordering is observed again in the Cu concentration range ( $x = 0.6 - 0.8$ ) [11], see Fig. 3.5.

Both DyNiAl and DyCuAl compounds orders ferromagnetically below  $T_C = 31$  K and 28 K [5, 12]. They also show a second magnetic phase transition characterized by the appearance of an antiferromagnetic component of spins in the basal plane below the temperatures of 15 K and 12 K. In the DyNi<sub>1-x</sub>Cu<sub>x</sub>Al series the step in lattice parameters is observed too (for  $x = 0.3 - 0.4$ ). Stronger antiferromagnetic ordering, on count of the ferromagnetic one, appears just for small part of Cu in DyNi<sub>1-x</sub>Cu<sub>x</sub>Al ( $x = 0.2$ ), later ( $x = 0.4$ ), only the antiferromagnetic component in the basal plane is present. Long-range

order disappears around  $x = 0.8$ . Above this concentration, the development of DyCuAl like long-range magnetic order occurs [13].

The disappearance of long-range magnetic order in all of the studied  $RNi_{1-x}Cu_xAl$  compounds was subject of further studies, including e.g. the muon spectroscopy [14].

The AC susceptibility measurements on  $NdNi_{1-x}Cu_xAl$  [15] and  $DyNi_{1-x}Cu_xAl$  [16] revealed frequency dependent maxima, typical for spin-glass systems. The concentration region of the long-range ordering loss and spin-glass behavior is between  $x = 0.6$  and  $x = 0.8$  for  $R = Tb, Dy$  or  $Er$ , but it is much wider ( $x$  between 0.4 and 0.8) for the Nd-based series [15].

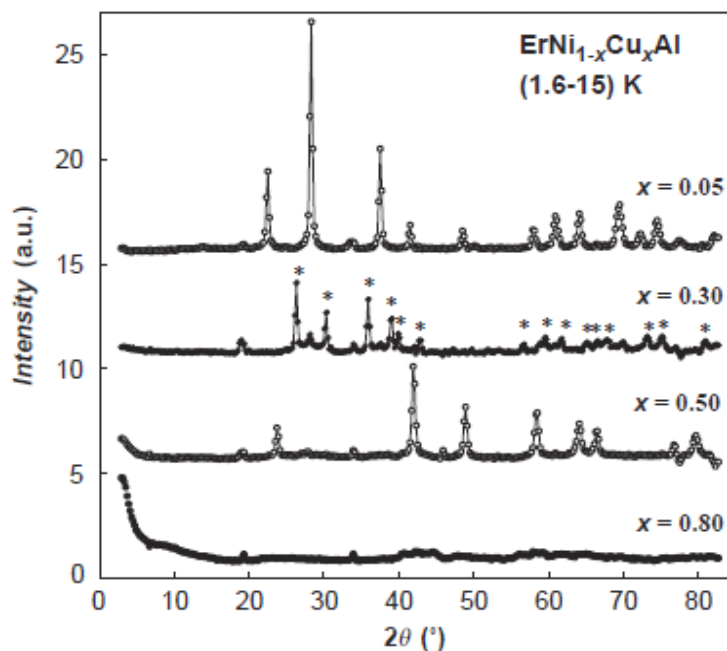


Fig. 3.5.: Powder neutron diffraction patterns of the  $ErNi_{1-x}Cu_xAl$  series [1]. The plotted intensities correspond to difference between the ordered and the paramagnetic state. Patterns belonging to different compounds are for better view shifted by 5 a.u. The loss of long range order occurs for  $x = 0.8$ .

## 4. Experimental methods

In this section all the experimental methods and procedures related with sample preparation are described. All measurements were performed in facilities of Department of Condensed Matter Physics, Charles University in Prague. Powder neutron diffraction experiment was performed in the Institute Laue-Langevin (ILL) in Grenoble.

### 4.1. Sample preparation

Our polycrystalline samples were prepared from pure elements by mono-arc melting. Elements with high purity Pr (99.9 %), Ni (99.995 %), Cu (99.999 %), Al (99.999 %) were used to ensure the best quality and correct stoichiometric compositions of final compounds. The mass of prepared samples was 2 - 5 g, the sample for neutron diffraction had the mass of  $\approx 20$  g.

At first the mono-arc oven was evacuated and then filled up by protective argon atmosphere at the pressure of approximately 0.6 bars. After the initial melting the procedure was repeated for a few times to achieve a good homogeneity of the samples. Evaporation pressure is relatively low for all of the used elements, namely at the temperature of 2000 K [19]: Pr (14 Pa), Ni (19 Pa), Cu (440 Pa), Al (650 Pa). Hence the amounts for melting were accurately weighted out according to desired stoichiometries. Relative mass loss during the melting was less than 1 %.

It should be mentioned that the most of the samples started to break down at the ambient pressure after a few weeks from the preparation. This effect is marginal in samples with smaller part of copper and seems to vanish only in case of  $\text{PrNi}_{0.3}\text{Cu}_{0.7}\text{Al}$ , which has kept its original shape for more than one year after the preparation.

### 4.2. Powder X-ray diffraction

Powder X-ray diffraction experiments were performed on diffractometer Bruker. The Bragg-Brentano conventional  $\theta$ - $2\theta$  geometry was used. The diffraction data were collected in the angle range of 10 - 80 degrees with the step of 0.05 degrees. The polycrystalline samples were crushed into powder, placed on a silicon tablet and radiated by Cu  $K_\alpha$  radiation with the wavelength of 1.5405 Å. Divergence slits of the diffractometer were kept fixed on the size of 6×6 mm. From that reason the measured intensities had to be

divided by the factor of  $\sin \theta$ . Diffraction patterns were evaluated by the Fullprof refinement program [20] using Rietveld single function fitting.

#### 4.3. Microprobe analysis

Microprobe analysis was done by scanning electron microscope Bruker. Task of this measurement was a determination of chemical compositions of impurity phases and their localization in the compound volume.

This measurement method puts big demands on flatness of the measured surface. For that purpose there were used special smoothing wheels covered with grinding substance. Surfaces of samples were ground by those wheels before putting the samples into the electron microscope.

#### 4.4. Neutron diffraction

The neutron diffraction experiment was performed on the D1B instrument in ILL in Grenoble. The powder sample was put into a vanadium container and irradiated by neutrons with the wavelength of 2.524 Å. The diffraction patterns were taken in the angle interval of 3.5 - 83.3 degrees and measured for two temperatures: 20 K (paramagnetic state) and 1.3 K (state of possible magnetic order). The measured patterns were, like in the case of X-rays, evaluated by the Fullprof program [20] using Rietveld single function fitting.

#### 4.5. Specific heat measurements

Specific heat was measured by the relaxation method on the PPMS (Physical Property Measurement System) 14 T and PPMS 9 T instruments in the Joint Laboratory for Magnetic Studies. Sample pieces ( $\approx 7$ -17 mg) were placed on a measuring puck, covered by a small amount of Apiezon N to ensure a good thermal contact between the sample and the puck. At the beginning the heat capacity of the addenda (puck + particular amount of Apiezon) was measured separately before inserting the sample and then subtracted from the data measured with the sample. The specific heat was measured in the temperature range 2-100 K in the zero magnetic field and additionally between 2 and 20 K in magnetic fields of 2 and 4 T.

#### 4.6. Measurements of magnetization

Magnetization measurements were performed on the PPMS and MPMS (Magnetic Property Measurement System) instruments. There were measured both DC magnetization and AC magnetization. Powder samples (with the mass around 100 mg) were placed into plastic ampoules and stuck up by special glue. Then it was fixed in the certain position in a plastic straw and placed on a sample holder of the instrument.

##### 4.6.1. DC magnetization measurements

Measurement of DC magnetization in dependence on temperature was performed in the temperature region 2-300 K. For temperatures 2-10 K with speed of heating 0.2 K/min and magnetic fields of 0.03 T, 0.1 T and 0.5 T both zero field cooled and field cooled dependencies were measured. In the temperature region between 10 and 300 K the temperature change speed was 1 K/min and magnetic fields 2 and 4 T. Dependencies of magnetization on applied magnetic field were measured at 2 K for magnetic fields 0-14 T with change of the field 0.01 T/sec. In temperatures 4.5 K, 8 K and 15 K it was measured for magnetic fields 0-7 T with the same speed.

##### 4.6.2. Measurements of AC susceptibility

AC susceptibility was measured on all samples to investigate a possible disappearance of long range ordering. Frequencies measured on PPMS: 13 Hz, 113 Hz, 1113 Hz and 9993 Hz. For samples with vanishing long range order there were measured an additional set of frequencies 43 Hz, 323 Hz, 643 Hz and on the instrument MPMS: 0.1Hz and 1Hz. Temperature regions were generally around 2.5-8 K interval. The cooling or heating speed was 0.1 K/min in all measurements of AC susceptibility.

For counting of the units in plots containing  $\chi_{AC}$  (section 5.3.2.) we used the classical calculation by  $M/H$  where  $H$  was the amplitude of the exciting magnetic field.

## 5. Results and discussion

### 5.1. Crystal structure

#### 5.1.1. X-ray diffraction

X-ray diffraction was performed in order to obtain the lattice parameters,  $c/a$  ratios and molar volumes. All measurements were performed on powder samples and analyzed in the way described in section 4.2. using the Fullprof program. Results of those measurements are summarized in Table 5.1.

Table 5.1.: Lattice parameters and volume of unit cell per formula unit of  $\text{PrNi}_{1-x}\text{Cu}_x\text{Al}$  series.

X	a (pm)	c (pm)	c/a	volume (nm <sup>3</sup> )
0.00 [32]	700.3(2)	408.5(2)	0.5833	0.05783
0.05	704.5(4)	408.9(3)	0.5804	0.05859
0.10	704.9(7)	409.0(5)	0.5802	0.05867
0.20	705.2(8)	409.2(7)	0.5803	0.05874
0.30	707.6(4)	410.3(3)	0.5799	0.05930
0.40	709.3(5)	410.9(4)	0.5793	0.05968
0.50	710.8(4)	411.4(3)	0.5788	0.06000
0.60	712.4(4)	412.0(3)	0.5783	0.06036
0.70	713.9(6)	412.5(4)	0.5778	0.06069
0.80	715.6(4)	413.1(3)	0.5773	0.06107
0.90	715.5(5)	414.2(4)	0.5789	0.06121
1.00 [2]	717.1(3)	414.8(1)	0.5784	0.06158

For all of the samples there were non indexed peaks in the diffraction patterns. This shows on the presence of impurity phases in the samples. Therefore all the samples were put into evacuated glass ampoules and annealed for a few weeks at temperature around 1000 K. Diffraction patterns of  $\text{PrNi}_{0.9}\text{Cu}_{0.1}\text{Al}$  before and after annealing are in Fig. 5.1. As one can see some of impurity phases reflections were notably cut back after the annealing. On the other hand a few reflections with no expected Bragg positions raised after annealing. They probably belong to some oxides mentioned in section 5.1.2. That is why, among others, the microprobe analysis was also performed to estimate origin of these impurity peaks.

The evolution of the lattice parameters and of the unit cell volume in dependence on parameter  $x$  is in agreement with previous results on parent compounds  $\text{PrNiAl}$  and  $\text{PrCuAl}$ .

The volume is rising with higher content of copper. In Fig. 5.2., there is clearly visible that the structure gap in  $c/a$  ratio ( $\approx 0.565 - 0.573$ ) reported in some other  $\text{RNi}_{1-x}\text{Cu}_x\text{Al}$  series is not present here, the  $c/a$  values lie well above this gap in the whole  $\text{PrNi}_{1-x}\text{Cu}_x\text{Al}$  series.

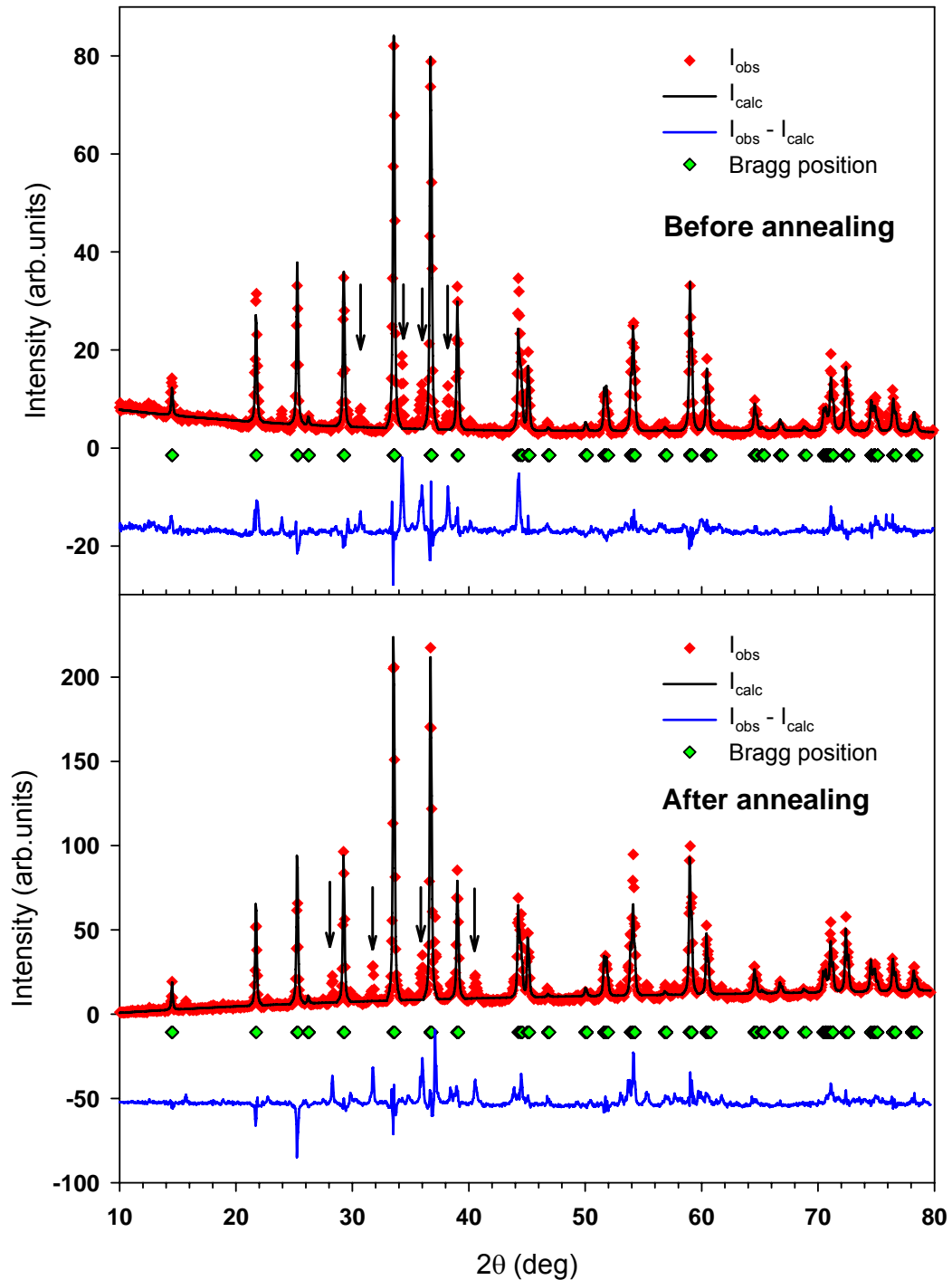


Fig. 5.1.: Diffraction patterns of  $\text{PrNi}_{0.9}\text{Cu}_{0.1}\text{Al}$  as cast sample and after the annealing. Arrows shows positions of impurity phases peaks with a significant intensity. Lines are plotted to guide the eye.

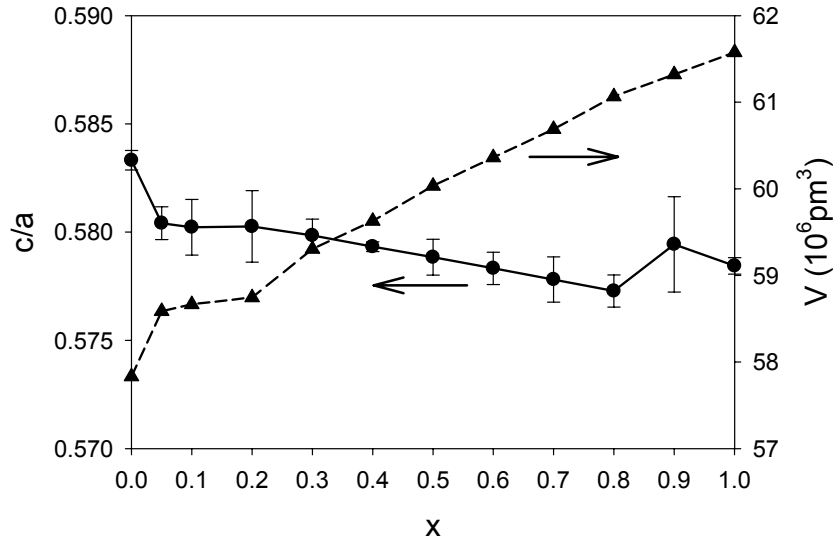


Fig. 5.2.:  $c/a$  ratios of lattice parameters and volume of the unit cell per formula unit of the  $\text{PrNi}_{1-x}\text{Cu}_x\text{Al}$  serie. Lines are plotted to guide the eye.

### 5.1.2. Microprobe analysis

The microprobe analysis was performed on  $\text{PrNi}_{0.9}\text{Cu}_{0.1}\text{Al}$  and  $\text{PrNi}_{0.3}\text{Cu}_{0.7}\text{Al}$  samples. For both samples there were investigated impurity phases present in the material. The amount of each phase was estimated by a graphical identification of their area in comparison with complete measured area using Adobe photoshop software. For better statistics, wider pictures of surfaces were made ( $175 \times 175 \mu\text{m}$  and  $330 \times 330 \mu\text{m}$  in case of  $\text{PrNi}_{0.9}\text{Cu}_{0.1}\text{Al}$  and  $\text{PrNi}_{0.3}\text{Cu}_{0.7}\text{Al}$ , respectively). Characteristic emission spectra were used for an identification of each element in the impurity phases. After subtraction of bremsstrahlung radiation (Fig. 5.3.), the instrument program also calculated stoichiometry of phases from these data. All results of the microprobe analysis are summarized in Table 5.2. Photos of the surfaces with pointers marking each impurity phase are included in Figs. 5.4. and 5.5.

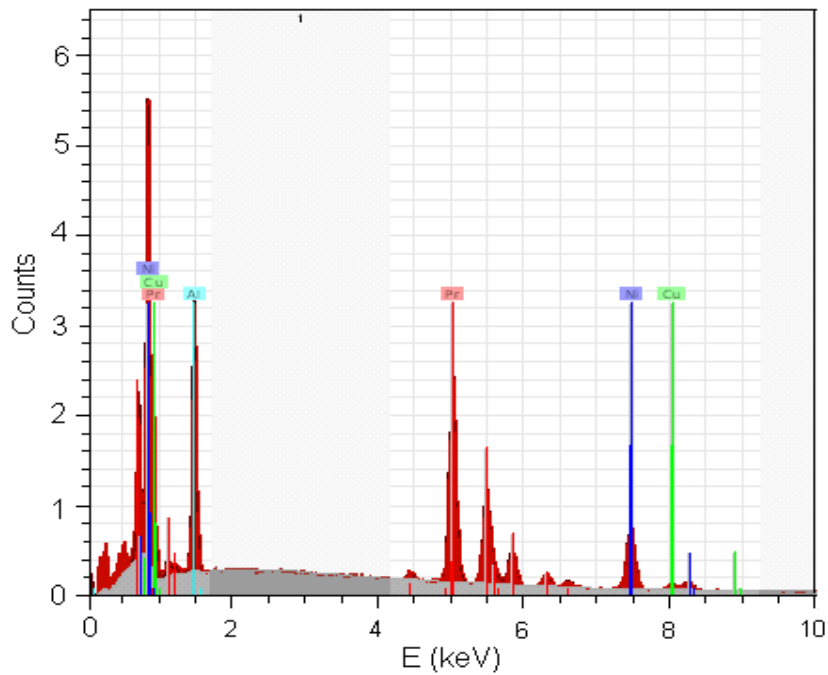


Fig. 5.3.: characteristic emission spectra of the main phase in  $\text{PrNi}_{0.9}\text{Cu}_{0.1}\text{Al}$ . Two gray bands are areas excluded from counting of bremsstrahlung radiation which is shown as the gray zone on the bottom side of the peaks.

Table 5.2.: Microprobe analysis summary for  $\text{PrNi}_{0.9}\text{Cu}_{0.1}\text{Al}$  and  $\text{PrNi}_{0.3}\text{Cu}_{0.7}\text{Al}$ .

$\text{PrNi}_{0.9}\text{Cu}_{0.1}\text{Al}$	Fraction	Pr	Ni	Cu	Ni+Cu	Al	O	Ta
Main phase	95.9%	0.307	0.318	0.045	0.363	0.331	0.000	0.000
Impurity phase 1	3.3%	0.214	0.305	0.076	0.381	0.405	0.000	0.000
Impurity phase 2	0.4%	0.314	0.000	0.000	0.000	0.000	0.686	0.000
Impurity phase 3	0.3%	0.172	0.000	0.000	0.000	0.000	0.828	0.000
Impurity phase 4	0.1%	0.000	0.000	0.000	0.000	0.000	0.000	1.000
$\text{PrNi}_{0.3}\text{Cu}_{0.7}\text{Al}$	Fraction	Pr	Ni	Cu	Ni+Cu	Al	O	Ta
Main phase	96.2%	0.300	0.107	0.258	0.365	0.335	0.000	0.000
Impurity phase 1	3.1%	0.143	0.058	0.423	0.481	0.377	0.000	0.000
Impurity phase 2	0.3%	0.303	0.017	0.163	0.180	0.519	0.000	0.000
Impurity phase 3	0.3%	0.169	0.000	0.000	0.000	0.000	0.830	0.000
Impurity phase 4	0.1%	0.000	0.000	0.000	0.000	0.000	0.000	1.000

Beside  $\text{PrNi}_{1-x}\text{Cu}_x\text{Al}$  phases having different stoichiometry from the one desired, praseodymium oxides in lower quantity were present in the samples and very small amount of Tantalum. The presence of Tantalum was probably caused by pollution of grinding wheels from previous sample surface smoothing before the preparation of our samples.

Following images contain measured surfaces. Comparing Fig. 5.4.a) and Fig. 5.5.a), one can see that in case of  $\text{PrNi}_{0.9}\text{Cu}_{0.1}\text{Al}$  the impurity phase 1 is concentrated in some bands likely corresponding to dislocations or grain boundaries. By contrast,  $\text{PrNi}_{0.3}\text{Cu}_{0.7}\text{Al}$  has its largest impurity phase joint to bigger volume clusters.

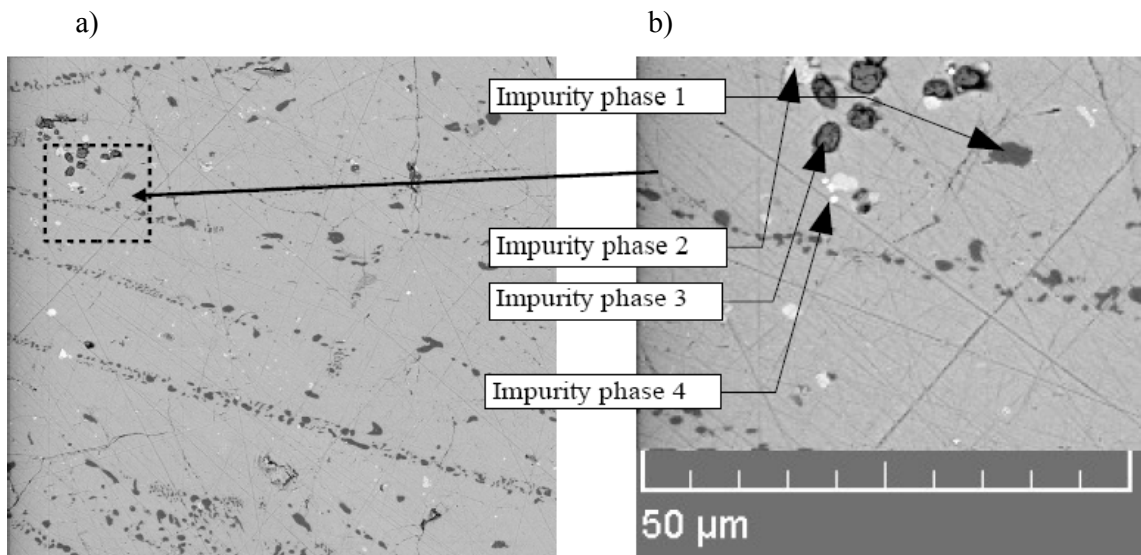


Fig. 5.4.: Microprobe analysis of  $\text{PrNi}_{0.9}\text{Cu}_{0.1}\text{Al}$ . Figure 5.4. a) shows the area used for the impurity phases fraction amount estimation. Figure 5.4. b) shows zoomed part used for impurity phases analysis.

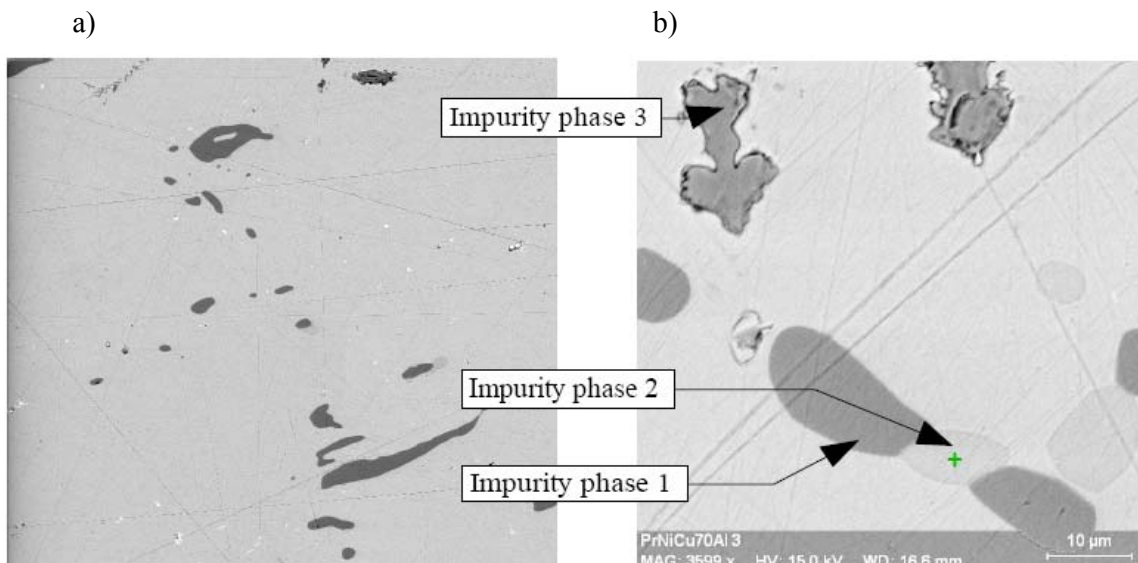


Fig. 5.5.: Microprobe analysis of  $\text{PrNi}_{0.3}\text{Cu}_{0.7}\text{Al}$ . Figure 5.5. a) shows the area used for the impurity phases fraction amount estimation. Figure 5.5. b) shows zoomed part (taken from a different picture than the one in figure 5.5. a)) used for impurity phases analysis.

## 5.2. Paramagnetic region

The  $M/H(T)$  dependencies in the temperature range between 10 K and the room temperature were measured for all of the prepared samples. They exhibit the typical Curie-Weiss behavior in the whole series.

For all of the compounds the measurements were carried out during both heating and cooling of the samples in the presence of magnetic fields of 2 T and 4 T. The  $M/H$  vs.  $T$  curves show some dependence on the temperature history. The data obtained during the cooling are somewhat different than those obtained during the heating. On the other hand, the  $M/H$  data are field independent. As an explanation of this discrepancy, we are expecting that the samples did not have enough time for taking the equilibrium value of temperature with their vicinity due to the different location of system's platform thermometer and the measured sample, resulting in these nonidentical curves.

In order to obtain correct values of the coefficients in the formula (6), we took average temperatures related to same values of  $H/M$  and put them into the fitting procedure. The plots were fitted by the Sigma plot software using a weight reciprocal to the  $H/M$  values. The resulting parameters are summarized in Table 5.3., together with another results from the following sections. For a better lucidity, we are showing the original measured data for  $\text{PrNi}_{0.3}\text{Cu}_{0.7}\text{Al}$  only, see Fig. 5.6. In Fig. 5.7., there are only the averaged  $H/M$  dependencies for the rest of the series.

Table 5.3.: Results of fitting of  $H/M$  experimental values to formula (6) in the paramagnetic region.

$x$	$T_{\text{ord}}$ (K)	$\theta_p$ (K)	$\mu_{\text{eff}}$ ( $\mu_B$ )	$\chi_0 * 10^9$ ( $\text{m}^3/\text{mol}$ )	$M_{14T,2K}$ ( $\mu_B/\text{f.u.}$ )
0.0[33]	6.5	-23	3.80	-	-
0.1	5**	-9.0	3.58	1.3	1.20*
0.2	4.7	-11.6	3.50	5.1	1.39
0.3	3.4	-10.3	3.58	-1.9	1.48
0.4	4.6	-8.6	3.54	5.0	1.53
0.5	4.0	-5.9	3.57	2.4	1.66
0.6	3.8	-9.1	3.59	3.7	1.55
0.7	3.4	-4.0	3.48	7.5	1.65
0.8	3.8	-5.8	3.61	3.2	1.69
0.9	4.5	-5.2	3.66	-2.0	1.30*
1.0[2]	7.9	-0.7	3.54	-	-

\*value in the magnetic field of 7 T.

\*\*this compound has an additional magnetic phase transition below the temperature of 2.1 K.

The effective moment  $\mu_{\text{eff}}$  is in the range  $3.56 - 3.69 \mu_{\text{B}}$ . These values are close to the  $\text{Pr}^{3+}$  free ion value of  $3.58 \mu_{\text{B}}$ . Paramagnetic Curie temperatures are in the all cases negative which is a sign of prevailing antiferromagnetic interactions present in the paramagnetic state.

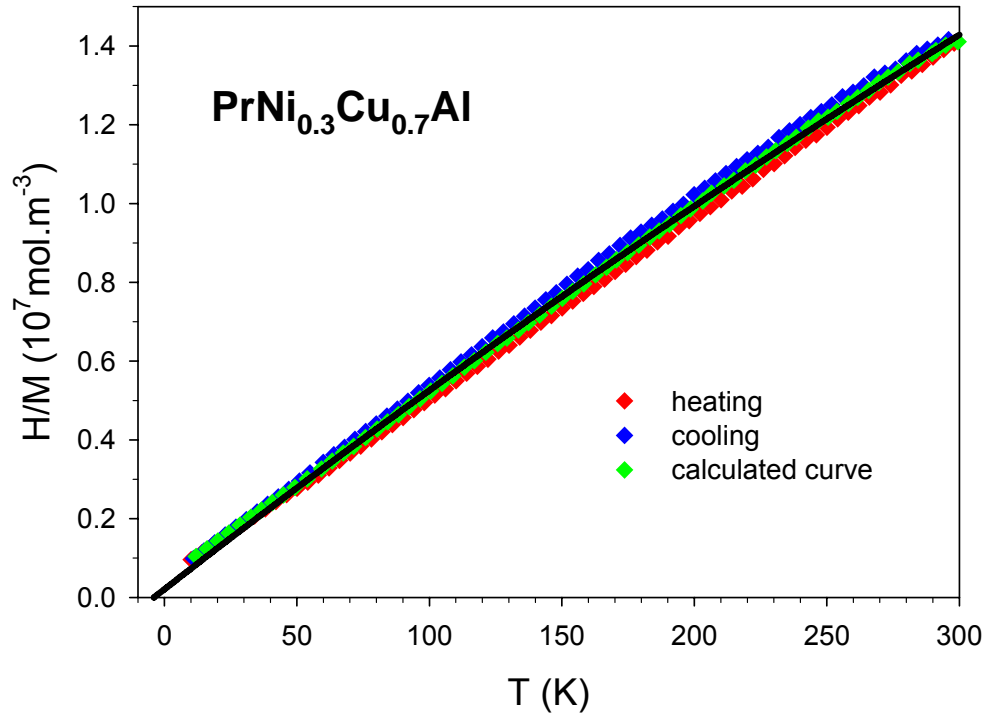


Fig. 5.6.: The original data measured on  $\text{PrNi}_{0.3}\text{Cu}_{0.7}\text{Al}$  during both cooling and heating. The counted curve (see text) which is in the middle, should best correspond to the real behavior of this compound. The black line results from fitting to the formula (6) with parameters included in Table 5.3.

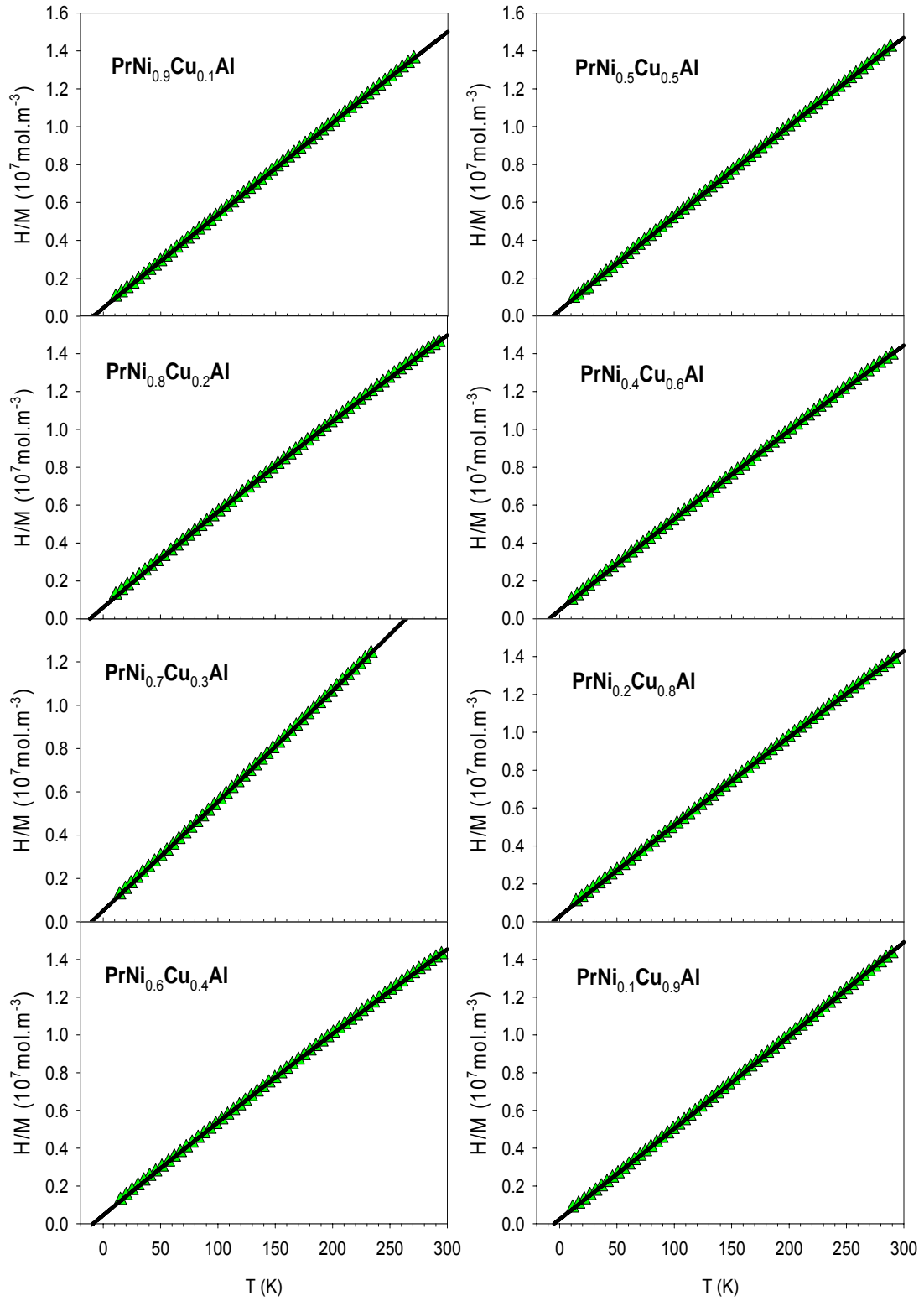


Fig. 5.7.: Temperature dependencies of the magnetization plotted as  $H/M$  vs.  $T$ . The data were measured in magnetic fields of 2 and 4 T. For a better lucidity, here we present only averaged data (see text). Black lines represent fit on eq. (6).

### 5.3. Magnetization measurements

In the following section we divided the series into two groups depending on the results consequential mainly from AC susceptibility measurements (see section 5.4.). The first group contains only the compounds which exhibit a long range magnetic ordering below its critical temperature ( $x = 0.1 - 0.4$ ), the second one includes the rest of the series ( $x = 0.5 - 0.9$ ).

#### 5.3.1. DC susceptibility

**$x = 0.1$**

The  $M/H(T)$  dependencies of  $\text{PrNi}_{0.9}\text{Cu}_{0.1}\text{Al}$  exhibit two anomalies at temperatures  $T = 5 \text{ K}$  and  $T = 2.1 \text{ K}$ , respectively, see Fig. 5.8. The anomaly at the lower temperature seems like one typical for a phase transition to an antiferromagnetic magnetic order with the same form of maximum for both FC and ZFC curves. By contrast, the anomaly at  $5 \text{ K}$  has a completely different shape for which it is not easy to distinguish if it is a sign of a transition into a ferromagnetic or an antiferromagnetic state.

Magnetization curves can be seen in Fig. 5.9. Higher the temperature is, lower is the related maximal value of magnetization appearing. That is quite a reasonable behavior as temperature makes magnetic moments fluctuate and thus cuts down the net magnetization. At the temperatures of  $2 \text{ K}$  and  $3 \text{ K}$  a metamagnetic transition appears above the magnetic field of  $4 \text{ T}$ . That is in good agreement with the previous results (see section 3.1.) on  $\text{PrNiAl}$  where a metamagnetic transition appeared in the magnetic field of  $6 \text{ T}$  at  $4.5 \text{ K}$ . An initial higher slope of curves in

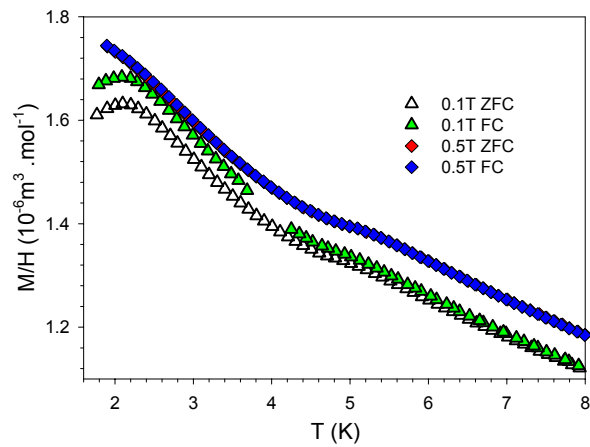


Fig. 5.8.:  $M/H(T)$  dependencies of  $\text{PrNi}_{0.9}\text{Cu}_{0.1}\text{Al}$ .

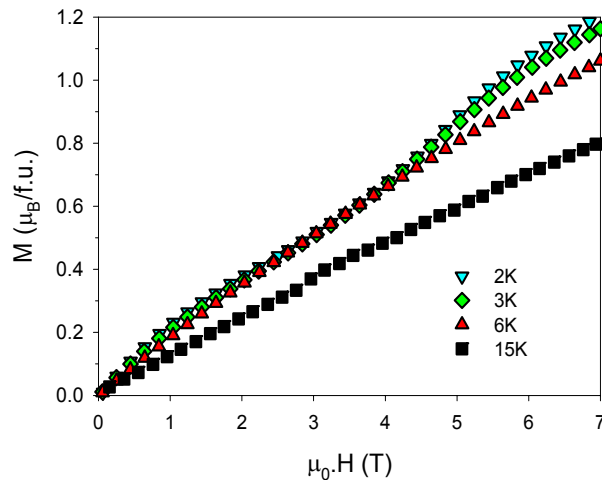


Fig. 5.9.: Magnetization dependencies of  $\text{PrNi}_{0.9}\text{Cu}_{0.1}\text{Al}$ . A metamagnetic transition occurs at  $4 \text{ T}$  in  $2 \text{ K}$  and  $3 \text{ K}$ .

those temperatures possibly shows on easy orientation of some antiferromagnetic component into the direction of magnetic field. In the temperature of 6 K, which is above a magnetically ordered state, any metamagnetic transition does not occur anymore. The same situation takes place in 15 K. The maximal value of magnetization in 7 T reaches  $1.2 \mu_B$  which is far from the  $\text{Pr}^{3+}$  value of  $3.2 \mu_B$ . This behavior is also similar to  $\text{PrNiAl}$  where the moment was not saturated even at the field of 35 T.

$$x = 0.2 - 0.4$$

The  $M/H(T)$  dependencies of  $\text{PrNi}_{0.8}\text{Cu}_{0.2}\text{Al}$ ,  $\text{PrNi}_{0.7}\text{Cu}_{0.3}\text{Al}$  and  $\text{PrNi}_{0.6}\text{Cu}_{0.4}\text{Al}$  will be discussed now. All these compounds have qualitatively same results, see Fig. 5.10.

All of the curves exhibit anomalies at temperatures approximately 4.7, 3.4 and 4.6 K for  $x = 0.2, 0.3$  and  $0.4$ , respectively. Those anomalies takes form of maxima in both zero field cooled and field cooled dependencies which shows on some kind of an antiferromagnetic order developing under the critical temperatures. That is similar to the parent compound  $\text{PrNiAl}$ . The irreversibility of ZFC and FC curves below the ordering temperatures occurs for all of these samples. It is probably caused by forming of domains during cooling in zero external field which reduces

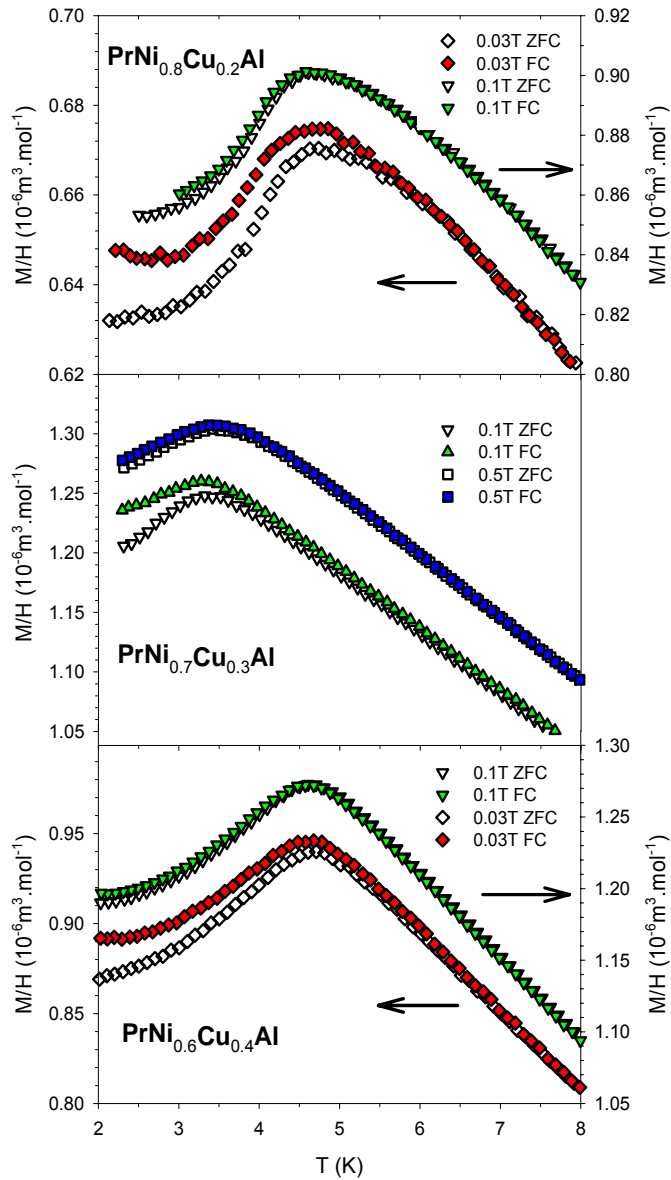


Fig. 5.10.:  $M/H(T)$  dependencies of  $\text{PrNi}_{1-x}\text{Cu}_x\text{Al}$ ,  $x = 0.2, 0.3, 0.4$ .

the net outer magnetization. By contrast, cooling in the presence of an external field makes the domains to orient in the field direction which partially increases the measured

magnetization. Of course, the bigger the applied field is, the smaller is the difference between the FC and ZFC dependence.

Magnetization curves of  $\text{PrNi}_{0.8}\text{Cu}_{0.2}\text{Al}$  (see Fig. 5.11.) are very similar to the ones of  $\text{PrNi}_{0.9}\text{Cu}_{0.1}\text{Al}$ . In this case a metamagnetic transition occurs in the field of 3 T. Again, in temperatures above the transition temperature, no metamagnetic transition can be observed.

An interesting situation takes place when we compare the results of  $\text{PrNiCu}_{0.7}\text{Cu}_{0.3}\text{Al}$  with the ones of  $\text{PrNiCu}_{0.6}\text{Cu}_{0.4}\text{Al}$ , see Fig. 5.12. Although, in case of the first one, it seems that there is no metamagnetic transition at all, for the second one a metamagnetic transition appears again in the field of 3 T at the temperature of 2 K. It can be due to a complicated magnetic structures of these compounds where the easy axes may often change their direction with the differing parameter  $x$ . In order to determine clearly these properties, one needs to measure single crystal samples instead of our polycrystalline ones.

The maximal values of magnetization are summarized in Table 5.3. (together with the rest of the series). On the first sight there is clear that they also hardly reach the maximum value for  $\text{Pr}^{3+}$  of  $3.2 \mu_B$ . That can be caused by the effect of crystal field which can favor a ground state where the orientation of magnetic moments reduces magnetization significantly. We also cannot expect that further metamagnetic transitions do not appear in higher applied fields.

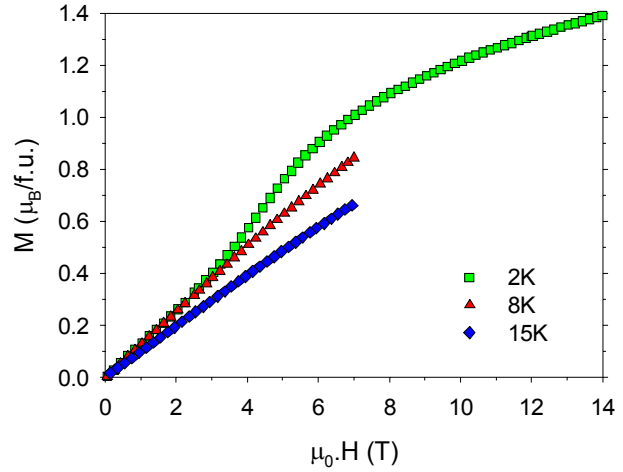


Fig.5.11.: Magnetization curves of  $\text{PrNi}_{0.8}\text{Cu}_{0.2}\text{Al}$ . Metamagnetic transition occurs at 3T in the temperature of 2K.

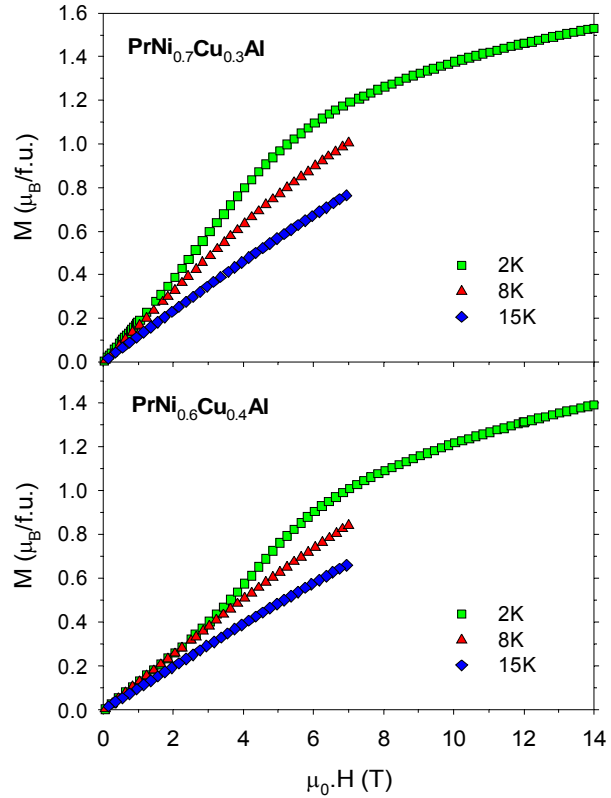


Fig. 5.12.: Magnetization curves of  $\text{PrNi}_{0.7}\text{Cu}_{0.3}\text{Al}$  and  $\text{PrNi}_{0.6}\text{Cu}_{0.4}\text{Al}$ . Metamagnetic transition occurs at 3T in the temperature of 2K for the latter one.

$$x = 0.5 - 0.9$$

All of the compounds from this set have similar curves of  $M/H(T)$ , see Fig. 5.13. They are characterized by an occurrence of broad anomalies below the transition temperatures which are 4, 3.8, 3.4, 3.8 and 4.5 K for  $x = 0.5, 0.6, 0.7, 0.8$  and  $0.9$ , respectively. Due to the enhanced flatness of the peaks, the determination of the critical temperatures from these curves is less accurate than it was in case of  $x = 0.1-0.4$ .

Again, the irreversibility between FC and ZFC curves appears but here it is considerably larger than in the previous group ( $x \leq 0.4$ ). It also nearly vanishes in the magnetic field of 0.5 T. Comparing these properties with

the previous results on the  $\text{ErNi}_{1-x}\text{Cu}_x\text{Al}$  series [32], where the enhanced irreversibility was connected with a loss of long range order in material, we can conclude (together with AC susceptibility results in the next section) that in our samples arises the same scenario. We note that the concentration region resulting from our measurements is wider than in case of heavy rare earth based  $\text{RNi}_{1-x}\text{Cu}_x\text{Al}$  compounds. This is similar observation as in the  $\text{NdNi}_{1-x}\text{Cu}_x\text{Al}$  series [15]. The application of higher magnetic field additionally causes another slicking down of the anomalies.

Magnetization curves for this set of compounds are plotted in Fig. 5.14. A metamagnetic transition does not appear in any of these compounds. The maximal values of magnetization do not differ notably from the previous compounds ( $x < 0.5$ ) and are summarized in Table 5.3.

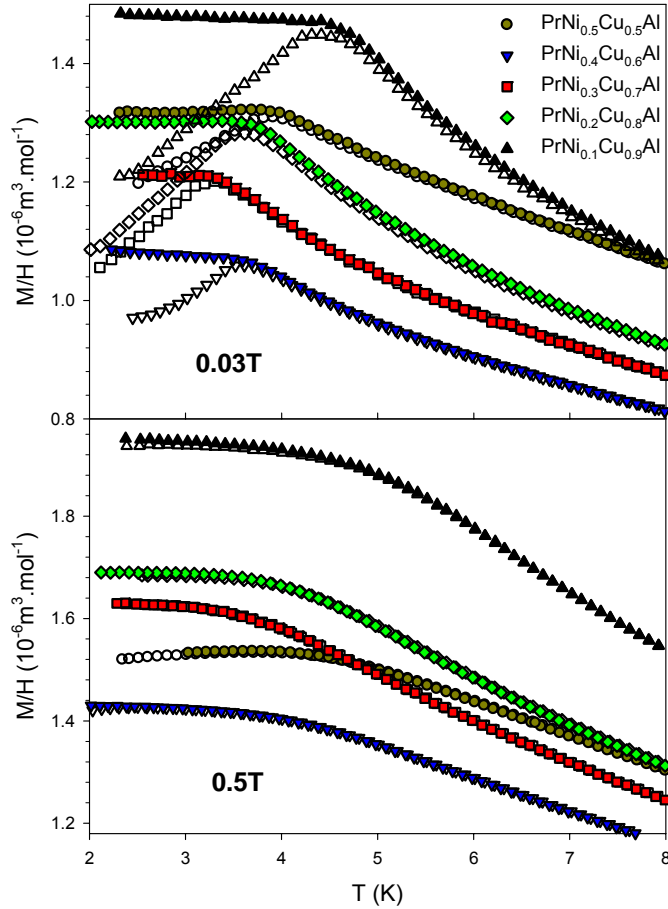


Fig. 5.13.:  $M/H(T)$  dependence for  $\text{PrNi}_{1-x}\text{Cu}_x\text{Al}$ ,  $x = 0.5 - 0.9$ , in magnetic fields of 0.03 and 0.5T, respectively. Full symbols identify FC measurement and bold symbols identify the ZFC measurement. Similarly to the previous set of compounds ( $x = 0.1 - 0.4$ ), the irreversibility between ZFC and FC curves nearly vanishes in the field of 0.5T. Additionally, the anomalies are even more flattened by the application of the higher magnetic field.

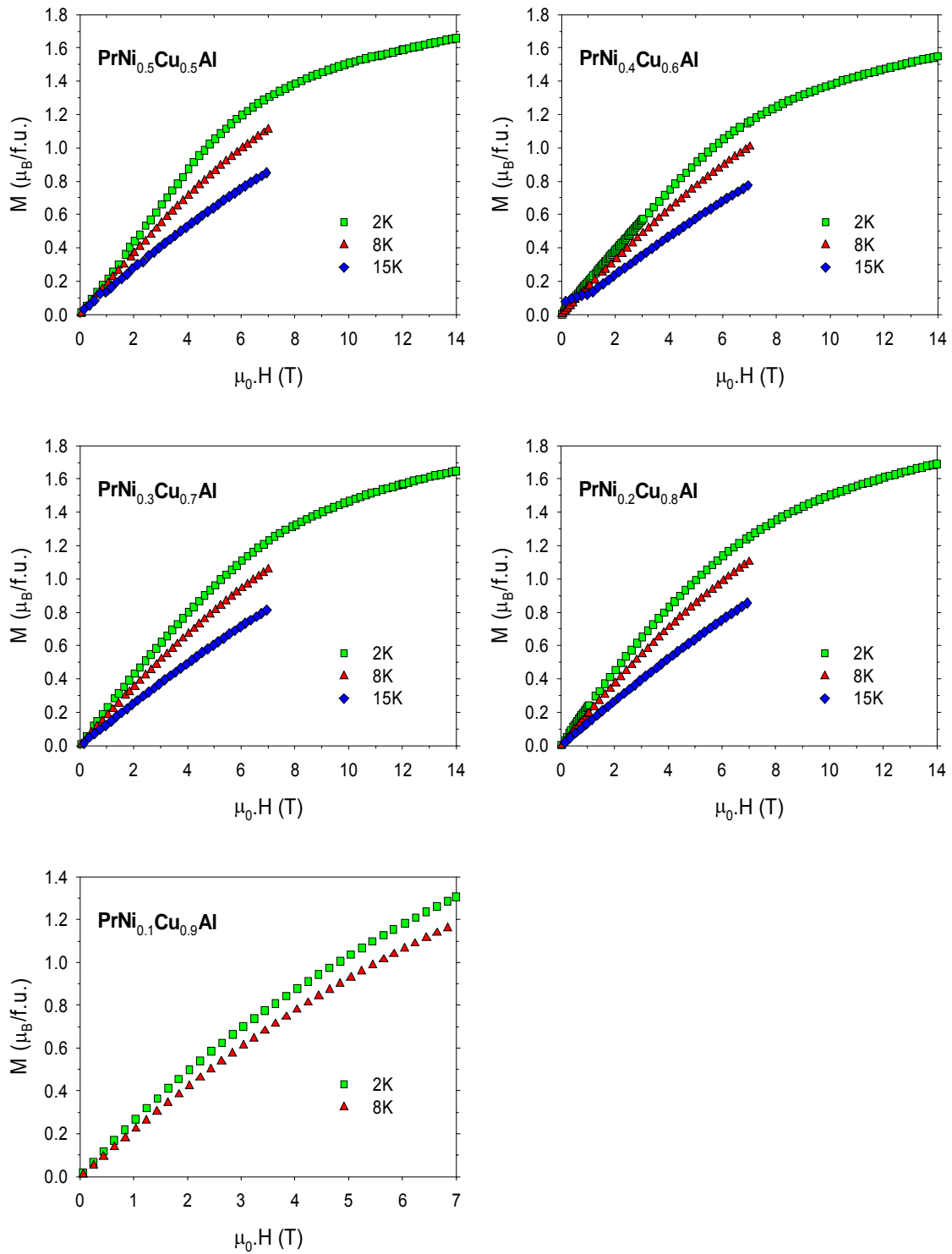


Fig. 5.14.: The magnetization curves of  $\text{PrNi}_{1-x}\text{Cu}_x\text{Al}$  for  $x = 0.5 - 0.9$ . Maximal values of magnetization are summarized in Table 5.3. No metamagnetic transition is observable for any of these compounds.

### 5.3.2. AC susceptibility

The main motivation for performing of the AC susceptibility measurement was the investigation of possible loss of long range magnetic order in  $\text{PrNi}_{1-x}\text{Cu}_x\text{Al}$ , similar to that reported in previous studies on other  $\text{RNi}_{1-x}\text{Cu}_x\text{Al}$  compounds (see section 3).

The results on the whole series reveal one clear maximum in the real part  $\chi_{AC}'$  and a small variety of behavior in the imaginary part  $\chi_{AC}''$ .

$$x = 0.2 - 0.4$$

These compounds were not expected to posses some interesting behavior in AC susceptibility since the  $M/H(T)$  dependencies indicated the existence of a long range magnetic order. This presumption is correct as one can see from Figs. 5.15. - 5.17. The temperature of maxima present in  $\chi_{AC}'$  curves are frequency independent and are well corresponding to the ordering temperatures determined from the  $M/H(T)$  measurements. For all of these samples the positions of maxima stays at the same temperature showing on frequency independent ordering temperature. That is typical behavior of long range ordered materials where the frequencies needed for the shifting are above the order of  $10^6$  Hz when the corresponding relaxation times are comparable with those of the inter spin relaxation processes. The imaginary part curves do not show any sign of a phase transition. The only exception is present in case of  $\text{PrNi}_{0.7}\text{Cu}_{0.3}\text{Al}$  where the  $\chi_{AC}''$  curves exhibit sudden enhancement below the ordering temperature.

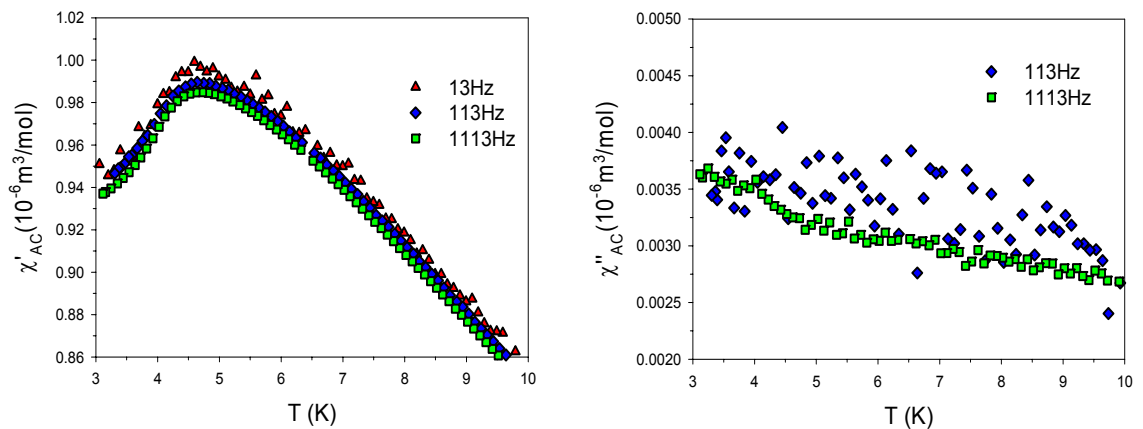


Fig. 5.15.:  $\chi_{AC}(T)$  dependencies of  $\text{PrNi}_{0.8}\text{Cu}_{0.2}\text{Al}$ . The maxima present in  $\chi_{AC}'$  curves stay at the same temperature for all measured frequencies. For the frequency of 13 Hz, the imaginary part curve has even more fluctuating behavior than it is in case of 113 Hz and, for a better lucidity, we do not plot it.

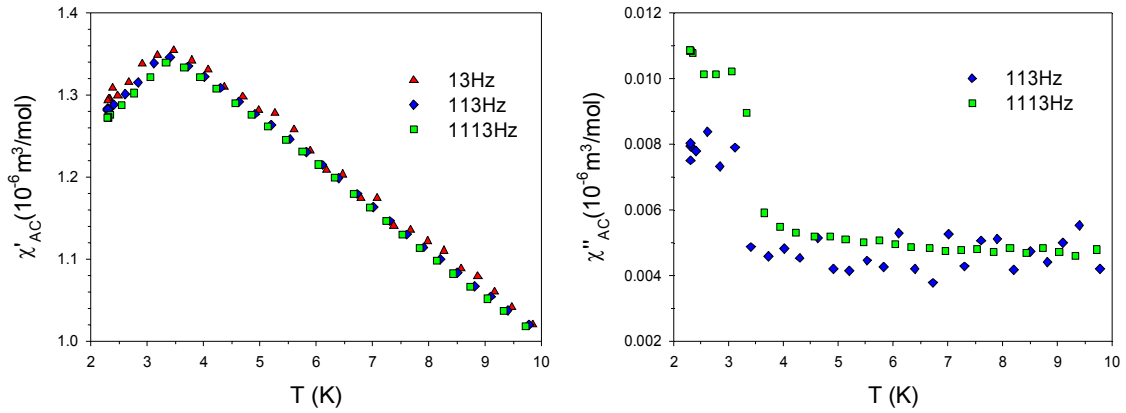


Fig. 5.16.:  $\chi_{AC}(T)$  dependencies of  $\text{PrNi}_{0.7}\text{Cu}_{0.3}\text{Al}$ . In the imaginary part, better distinguishable transition can be observed. The curve of 13 Hz frequency rapidly fluctuates and therefore is not plotted.

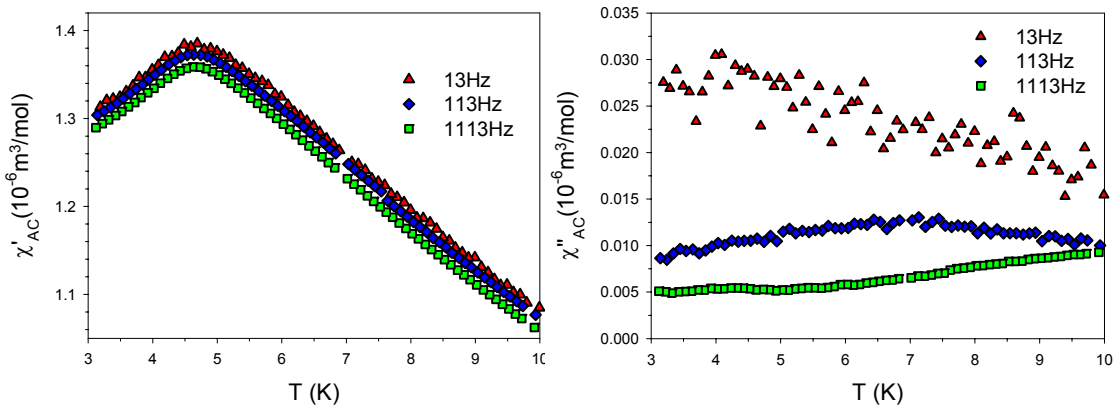


Fig. 5.17.:  $\chi_{AC}(T)$  dependencies of  $\text{PrNi}_{0.6}\text{Cu}_{0.4}\text{Al}$ .

### $x = 0.5 - 0.9$

On first sight, the real part curves have the same shape as the ones for  $x = 0.2 - 0.4$ . But, contrary to the first group, the positions of anomalies are evidently moving to higher temperatures with increasing frequency of the applied excitation field, see Figs. 5.18. and 5.19. This is a strong indication of absence of any long range magnetic order as was already explained in the previous paragraph. Hence the loss of long range order occurs also in case of the  $\text{PrNi}_{1-x}\text{Cu}_x\text{Al}$  series.

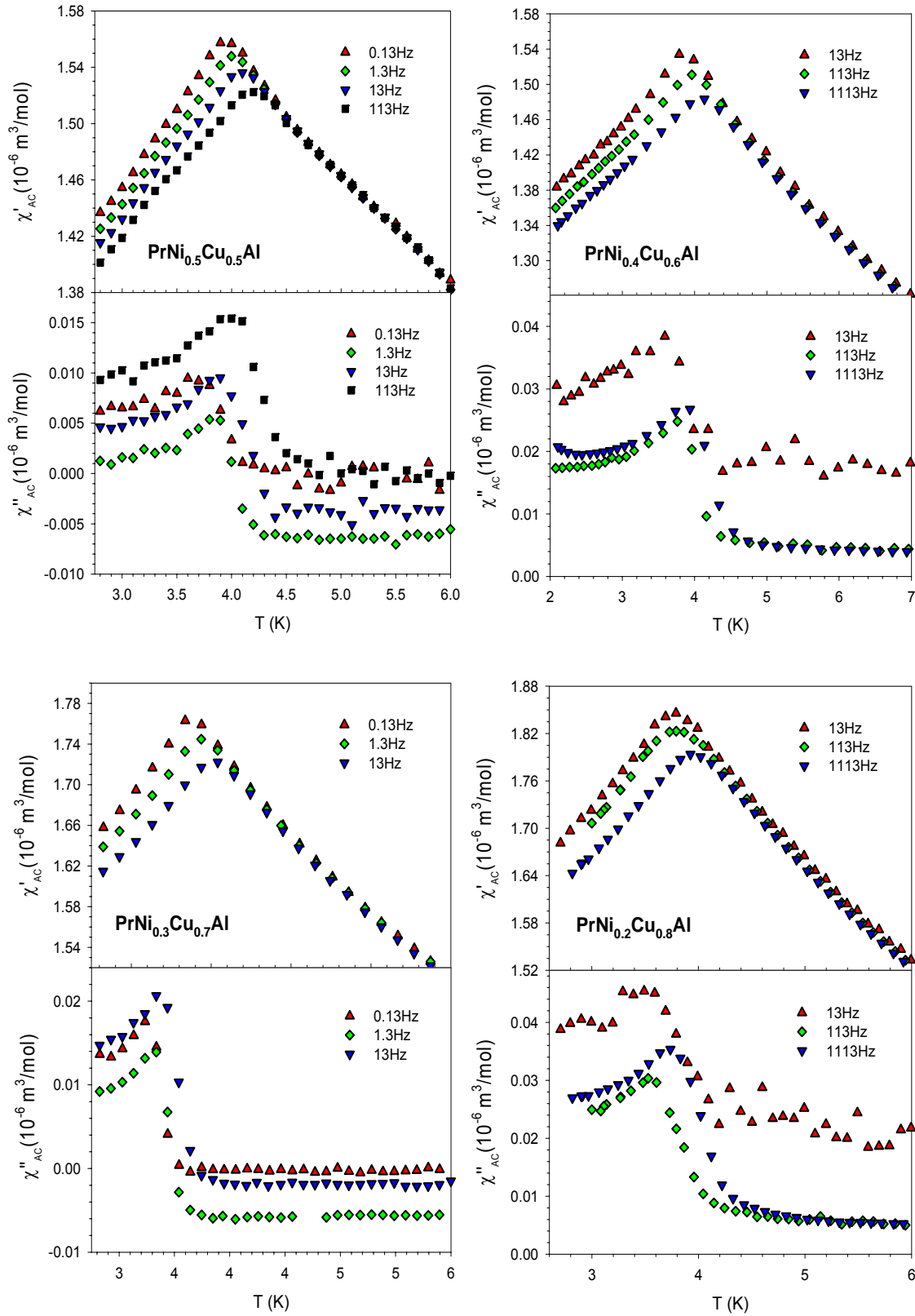


Fig. 5.18.:  $\chi_{AC}(T)$  dependencies of  $\text{PrNi}_{1-x}\text{Cu}_x\text{Al}$ ,  $x = 0.5 - 0.8$ . Clearly visible anomalies in both the real and the imaginary part are moving to higher temperatures with increasing frequencies.

To analyze these data more deeply we will use formulas (8) and (9) exerting the  $T_f$  temperatures which belong to the maxima in the  $\chi_{AC}'$  curves as these seem to be subtracted

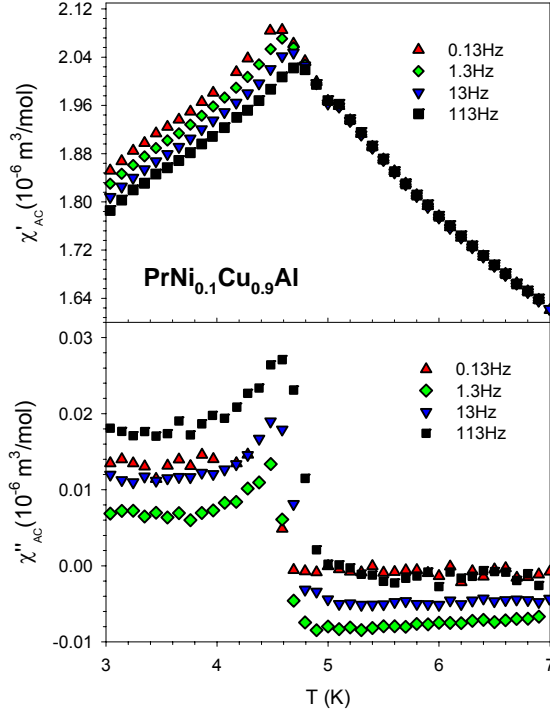


Fig. 5.19.:  $\chi_{AC}$  (T) dependencies of  $\text{PrNi}_{0.1}\text{Cu}_{0.9}\text{Al}$ .

The procedure was done for  $x = 0.5, 0.7$  and  $0.9$  because measurements on a wider frequency region were performed only on these compounds. The values of  $\delta T_f$  are  $0.009$  for  $\text{PrNi}_{0.5}\text{Cu}_{0.5}\text{Al}$  and  $0.006$  for both  $\text{PrNi}_{0.3}\text{Cu}_{0.7}\text{Al}$  and  $\text{PrNi}_{0.1}\text{Cu}_{0.9}\text{Al}$ . These values are slightly lower than in the results on the  $\text{DyNi}_{1-x}\text{Cu}_x\text{Al}$  series [ ] but are comparable to the results on some other metallic spin glass systems, e.g.  $\delta T_f = 0.010$  in  $\text{AuFe}$  (Mydosh, SG) which can be also evaluated using the Vogel-Fulcher law. Table 5.4. contains fitted parameters from the formula (8). The obtained  $E_A$  and  $T_{VF}$  values well correspond to the observed behavior. The activation energies between  $10$  and  $30$  K are quite reasonable since the freezing temperatures are around the temperature of  $4$  K.

more accurately than the anomalies in the imaginary part. The second of the formulas gives guidance how to treat the results (see section 2.1.4.). Taking a logarithm of the formula (8) grants us an opportunity to plot the  $T_f$  temperatures vs.  $1/\ln(f_0/f)$ , see Fig. 5.20. In these plots the direction of the plotted line corresponds to the value of the activation energy  $E_A$  and the interception with y-axis equals to the value of the related Vogel-Fulcher temperature. We keep the value of  $f_0$  fixed as the different approach would make the fit numerically unstable. A few different frequencies  $f_0$  from a range which is typical for spin glass systems are chosen.

Table 5.4.: Fitted parameters contained in the Vogel-Fulcher law. Several values of  $f_0$  were used and fixed as a parameter in the fit of the experimental data to the eq. (8).

	$f_0$ (Hz)	$10^{10}$	$10^{11}$	$10^{12}$	$10^{13}$	$10^{14}$
PrNi <sub>0.5</sub> Cu <sub>0.5</sub> Al	$E_A/k_B$ (K)	16	20	24	29	33
	$T_{VF}$ (K)	3.3	3.2	3.1	3.0	3.0
PrNi <sub>0.3</sub> Cu <sub>0.7</sub> Al	$E_A/k_B$ (K)	11	14	16	19	22
	$T_{VF}$ (K)	2.9	2.9	2.8	2.8	2.7
PrNi <sub>0.1</sub> Cu <sub>0.9</sub> Al	$E_A/k_B$ (K)	14	17	20	24	28
	$T_{VF}$ (K)	4.0	3.9	3.9	3.8	3.7

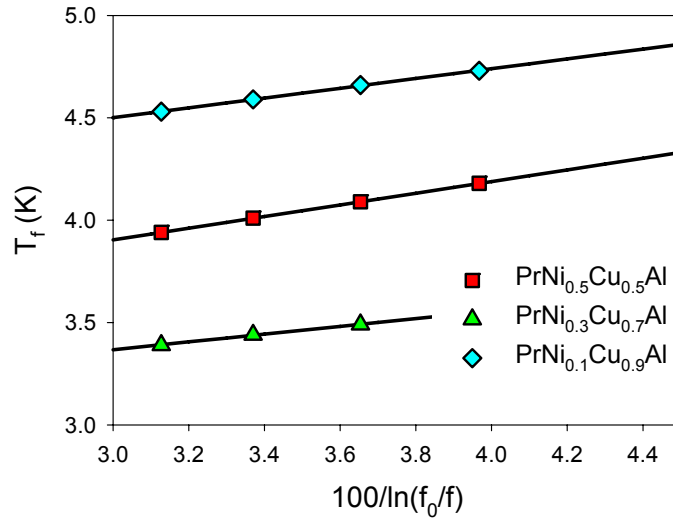


Fig. 5.20.: Fitting of the experimental data on PrNi<sub>1-x</sub>Cu<sub>x</sub>Al,  $x = 0.5, 0.7$  and  $0.9$ . The black lines are fitting curves of the Volger-Fulcher law. The  $f_0$  frequency is fixed on  $10^{13}$  Hz. The intercept with the y-axis gives value of  $T_{VF}$  and the slope of the curve determines the activation energy  $E_A$ .

AC susceptibility was also measured in presence of an external magnetic field. Generally, the results show that anomalies in both  $\chi_{AC}'$  and  $\chi_{AC}''$  are more broadened with increasing magnetic field, see Figs. 5.21. and 5.22. Up to the field of 0.03 T ( $x = 0.7 - 0.9$ ), the anomalies stay at the same temperatures, above 0.1 T ( $x = 0.8$ ), they are gradually moving to lower temperatures and almost vanish in 1 T, see Fig. 5.22.

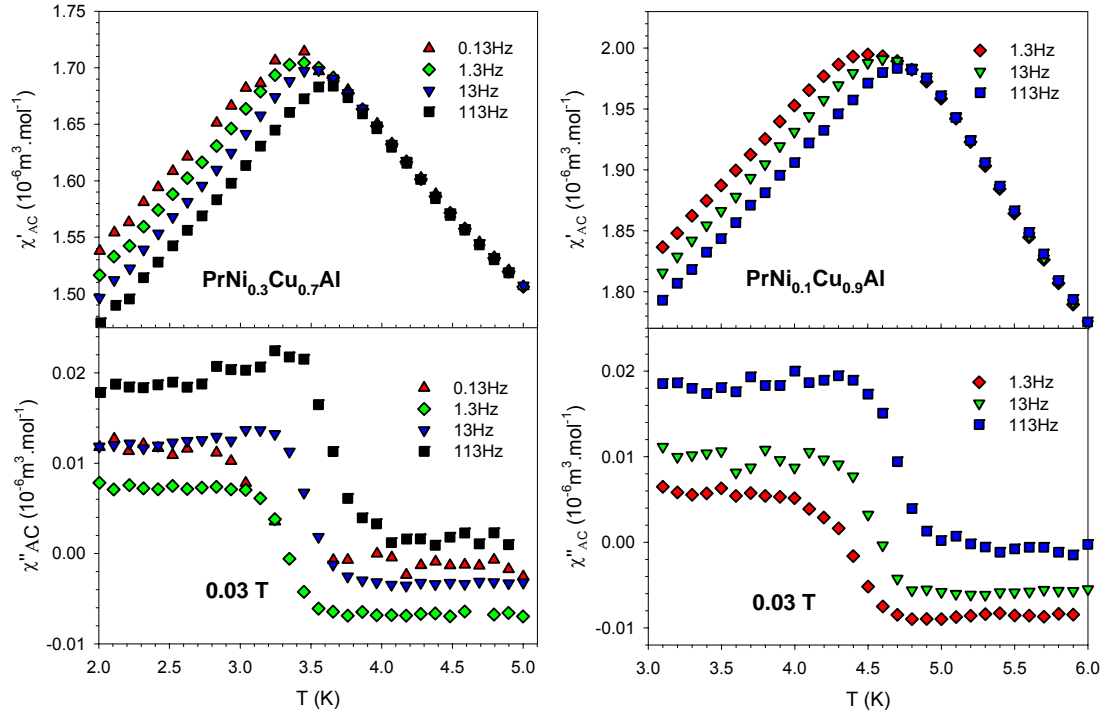


Fig. 5.21.:  $\chi_{AC}(T)$  dependencies of  $\text{PrNi}_{0.3}\text{Cu}_{0.7}\text{Al}$  and  $\text{PrNi}_{0.1}\text{Cu}_{0.9}\text{Al}$  in presence of the magnetic field of 0.03 T. The anomalies stay at the same temperatures as without the field but are more broadened.

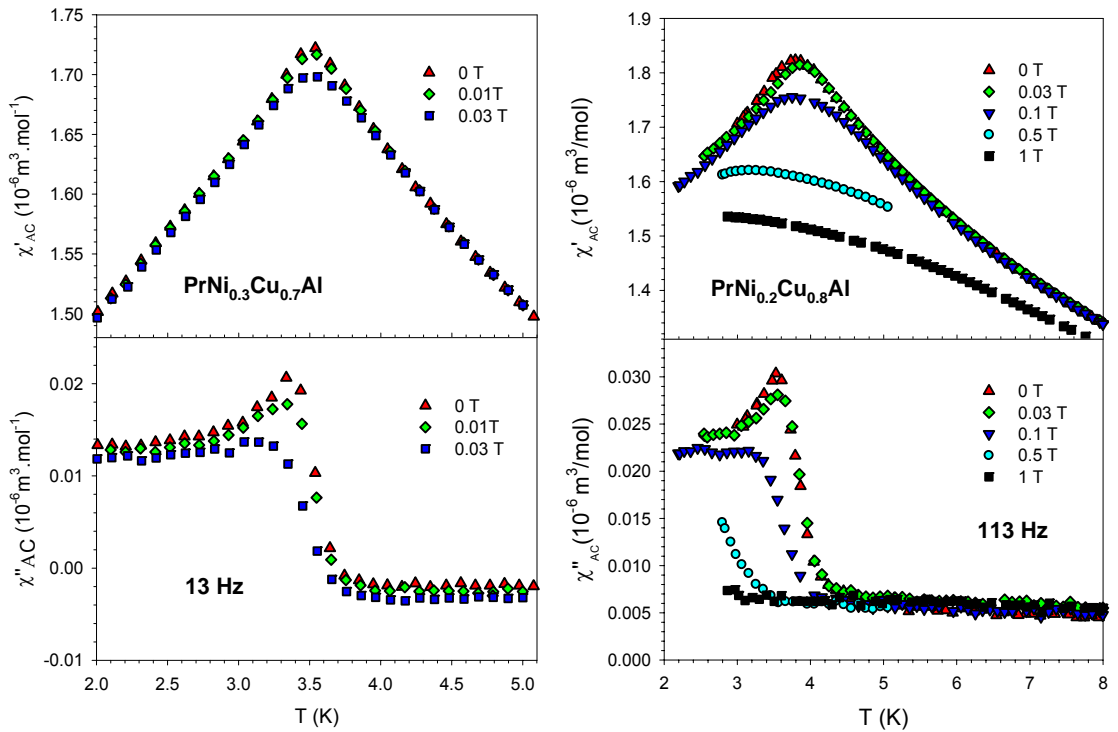


Fig. 5.22.:  $\chi_{AC}(T)$  dependencies of  $\text{PrNi}_{0.3}\text{Cu}_{0.7}\text{Al}$  and  $\text{PrNi}_{0.2}\text{Cu}_{0.8}\text{Al}$  measured in one frequency and different magnetic fields. As can be seen, with raising magnetic field the anomalies become more broadened. For fields up to 0.03 T the maxima stay in the same temperature. From the field of 0.1 T, the anomalies are moving to lower temperatures. Additionally, in the field of 1 T, the transition almost vanishes.

#### 5.4. Heat capacity measurements

The specific heat of the  $\text{PrNi}_{1-x}\text{Cu}_x\text{Al}$  compounds is shown in Fig. 5.23. In the high temperature region (above 20 K) of the  $C_p(T)$  curves we can see that the curves exhibit no anomalies and almost reach the classical limit value  $3n.R$  (here  $n = 3$ ) at 180 K. The specific heat of  $\text{LuNiAl}$  and  $\text{LuCuAl}$  [34] is also shown here for comparison. The specific heat of these two non-magnetic compounds is a sum of phonon and electronic contributions (see section 2.2.3.). The enhancement of the specific heat of praseodymium containing compounds can be generally contributed to the Schottky specific heat (see formula (17)) and possibly also to small differences in the phonon part.

In the low temperature region (below 20 K) specific heat measurements revealed anomalies which are located at the same temperatures as the ordering temperatures indicated by magnetization and AC susceptibility data, respectively, see insets in Fig. 5.23.

The possible phase transition at 2 K, observed in the  $M/H(T)$  curve of  $\text{PrNi}_{0.9}\text{Cu}_{0.1}\text{Al}$ , is not distinguishable here but some small anomaly can be traced out in Fig. 5.24. The increase in the curve starting below the temperature of 1 K is probably caused by a nuclear contribution of Pr atoms.

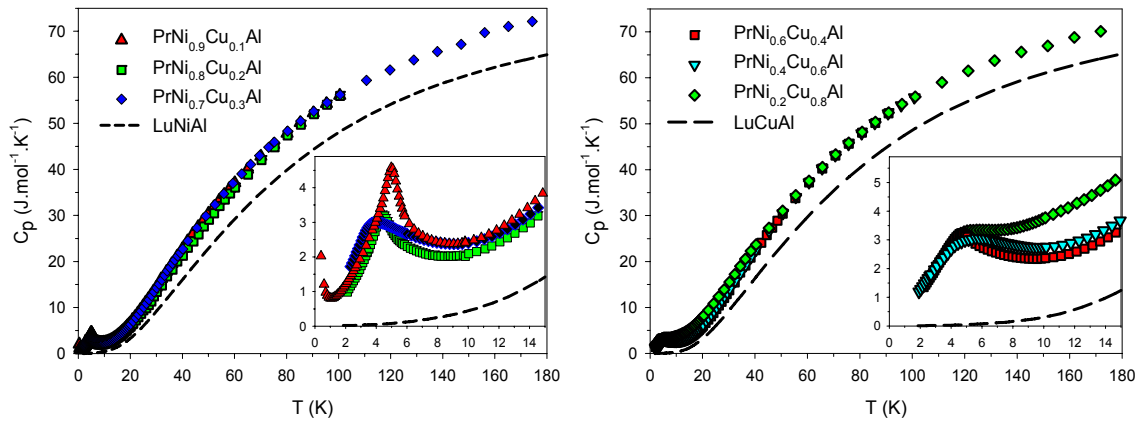


Fig. 5.23.: Specific heat curves of the  $\text{PrNi}_{1-x}\text{Cu}_x\text{Al}$  series,  $x = 0.1, 0.2, 0.3, 0.4, 0.6, 0.8$ , together with  $\text{LuNiAl}$  and  $\text{LuCuAl}$  compounds. Two small inset plots are showing the low temperature region where anomalies representing possible phase transitions are observable. No other singularities are present in any of the curves. For compounds with  $x = 0.1 - 0.4$ , the anomalies own typical shape of transition from a paramagnetic into a long range ordered state. In contrary, the rest of the series anomalies have their shape more broadened which was also reported in some other spin glass systems. The additional increase below 1 K in case of  $\text{PrNi}_{0.9}\text{Cu}_{0.1}\text{Al}$  is probably caused by a nuclear contribution of Pr atoms to the specific heat.

Again, the dependencies of the previously created two groups differ in shapes of anomalies. The anomalies in case of  $x = 0.6$  and  $0.8$  are broadened in comparison with those of  $x = 0.1 - 0.4$ . That reminds the broadening in  $M/H(T)$  curves which was present for these compounds ( $x = 0.5 - 0.9$ ) too. It originates from the progressive formation of spin clusters, resulting in the extension of specific heat dependencies. This effect had been also found in the  $\text{ErNi}_{1-x}\text{Cu}_x\text{Al}$  series [32] and in some other compounds exhibiting a spin glass state, e.g.  $\text{Ce}_2\text{CuSi}_3$  [35].

In the first approximation, we take the specific heat of the non-magnetic compounds  $\text{LuNiAl}$  (for  $x = 0.1 - 0.4$ ) and  $\text{LuCuAl}$  (for  $x = 0.6$  and  $0.8$ ) as an estimation of the phonon and the electron contributions in the  $\text{PrNi}_{1-x}\text{Cu}_x\text{Al}$  compounds. This approach is not very accurate because Lu is relatively far from Pr in the periodic table of elements. Consequently, we can see a discrepancy in the high temperature region where the Lu based and the Pr based compounds curves should be well consistent due to a dominant contribution of the phonon part. On the other hand, the procedure is a good approximation at the low temperature region where the phonon and electron contributions are relatively small. More suitable would be to take  $\text{LaNiAl}$  and  $\text{LaCuAl}$  as non-magnetic analogs, but both these compounds crystallize in the orthorhombic crystal structure which would lead to even higher discrepancy with respect to the  $\text{PrNi}_{1-x}\text{Cu}_x\text{Al}$  series.

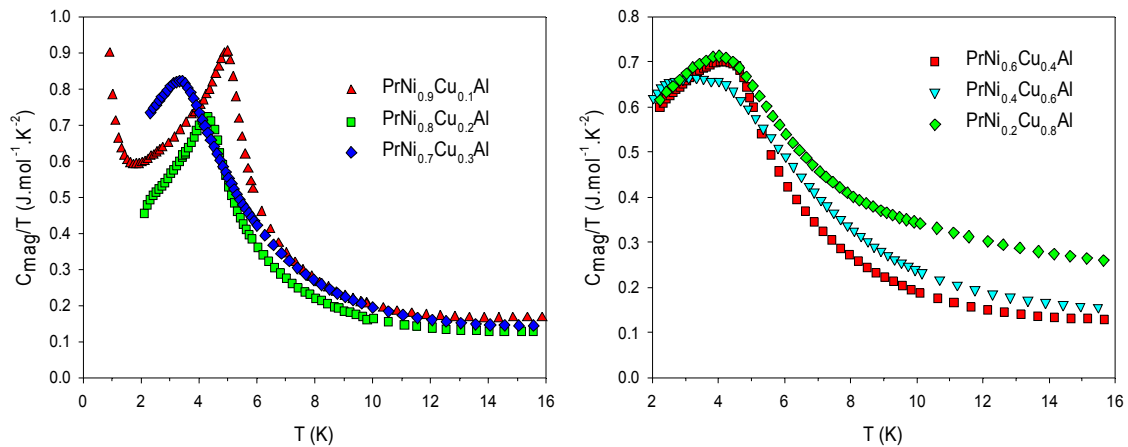


Fig. 5.24.: Magnetic specific heat of the  $\text{PrNi}_{1-x}\text{Cu}_x\text{Al}$  series,  $x = 0.1, 0.2, 0.3, 0.4, 0.6, 0.8$ , divided by temperature. The anomalies are discussed in the comment of Fig. 5.23. In case of  $\text{PrNi}_{0.9}\text{Cu}_{0.1}\text{Al}$  above 2 K, there is just a small bulge overlapped by the increase of specific heat due to the nuclear contribution for which it cannot be well distinguished. In the  $\text{PrNi}_{0.8}\text{Cu}_{0.2}\text{Al}$  curve there is probably also a sign of another phase transition near the temperature of 2 K having an inexpressive confirmation in the  $M/H(T)$  curve, see Fig. 5.10.

The  $C_{mag}/T$  vs.  $T$  data are plotted in Fig. 5.24. In the curve of  $\text{PrNi}_{0.8}\text{Cu}_{0.2}\text{Al}$  we can see a small bulge near the temperature of 2 K, similar to the one in the  $\text{PrNi}_{0.9}\text{Cu}_{0.1}\text{Al}$  curve. This anomaly has only inexpensive analogy in the  $M/H(T)$  curve, see Fig. 5.10. Therefore it cannot be interpreted reasonable now.

The data plotted in Fig. 5.24. gave us an opportunity to calculate amount of the entropy below the ordering temperature and to estimate the energies of further excited crystal field states using formulas (17) and (19). Since the dependencies are measured down to the temperature of 2 K, we linearly extrapolated the  $C_{mag}/T$  data from 2 K to the absolute zero temperature. That was done also in case of  $\text{PrNi}_{0.9}\text{Cu}_{0.1}\text{Al}$  compound which is measured down to 1 K but below the temperature of 2 K a nuclear contribution to the specific heat appears.

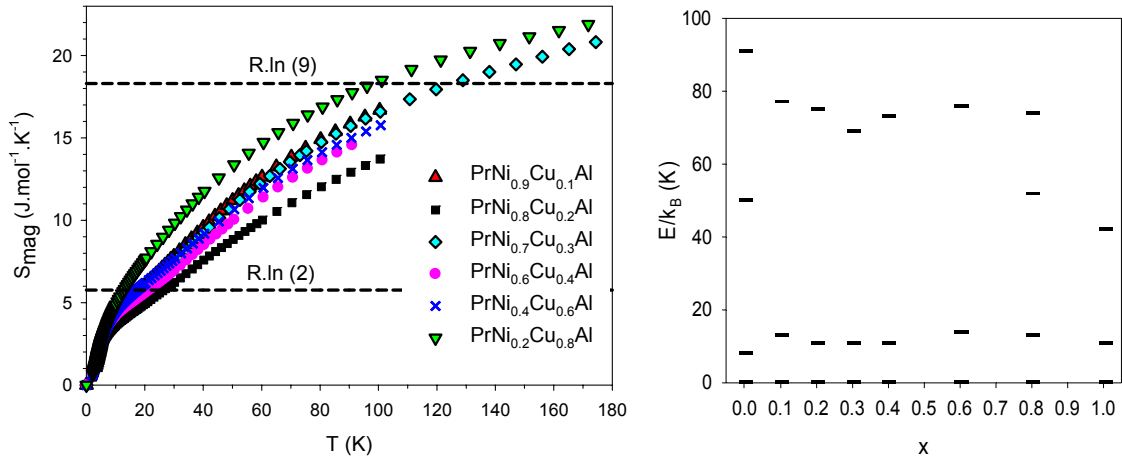


Fig. 5.25.: Calculated curves of the magnetic entropy and the estimated energy levels scheme in the  $\text{PrNi}_x\text{Cu}_{1-x}\text{Al}$  series. The energy level scheme is plotted only below 100 K, the estimation of higher levels is not reliable.

As we can see in Fig. 5.25., the magnetic entropy at the highest measure temperatures exceeds the value of  $R.\ln 9 = 18.3 \text{ J.mol}^{-1}.\text{K}^{-1}$  (the dashed line in the plot) obtained from the formula (20) considering the state with  $J = 4$  for  $\text{Pr}^{3+}$  ion as its ground state. This can be caused either by rough subtraction of the phonon and electron contributions using  $\text{LuNiAl}$  and  $\text{LuCuAl}$  specific heats or by an additional mixture of excited ionic states with the different value of  $J$ . We do not see the latter possibility as probable in our case. In the low temperature region the entropy is close to the value of  $R.\ln 2 = 5.76 \text{ J.mol}^{-1}.\text{K}^{-1}$  which shows on quasi-doublet ground state.

The estimation of the energy levels scheme from Schottky contribution can be performed using the formula (17) and is plotted in Fig. 5.25. It can be seen that in the energy

levels scheme there is no clear evolution in the series. The lowest laying quasi-doublet is well separated from the rest of the levels in the whole series. The data on the parent compounds PrNiAl and PrCuAl, shown also here, were determined from neutron diffraction [36] and specific heat measurements [2], respectively.

The fit on equation (19) was performed to data enough above the phase transition peaks and, depending on the selected compound, below the temperatures of approx. 70 K (due to the uncertainty of the phonon contribution), therefore we show only the levels below the temperature of 100 K. The fitting in case of PrNi<sub>0.8</sub>Cu<sub>0.2</sub>Al and PrNi<sub>0.2</sub>Cu<sub>0.8</sub>Al is shown in Fig. 5.26.

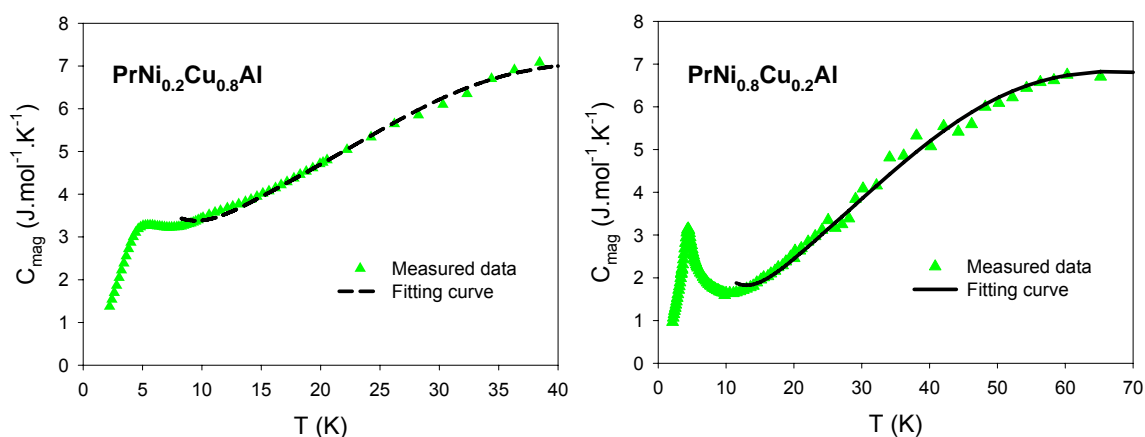


Fig. 5.26.: Fitting of the Schottky contribution of PrNi<sub>0.8</sub>Cu<sub>0.2</sub>Al and PrNi<sub>0.2</sub>Cu<sub>0.8</sub>Al.

The effect of applied magnetic field on the specific heat data is demonstrated on Fig. 5.27. In the  $C_{mag}/T$  ( $T$ ) dependence one can easily conclude whether a measured compound orders ferromagnetically or antiferromagnetically from the relative movement of the area below the peak of phase transition. The area corresponds to the amount of entropy. If it moves to lower temperatures in the presence of a magnetic field, the compound orders antiferromagnetically, and vice-versa in the opposite situation. Some sort of tendency can be observed. The antiferromagnetic order is clearly indicated for the  $x = 0.1$  compound. The entropy shifts gradually to lower temperatures for magnetic fields up to 6 T. In 8 T, the ferromagnetic order is partly induced (see also Fig. 5.9.), and we observe entropy shift to higher temperatures. The field needed to induce the ferromagnetic order decreases with increasing Cu content - it amounts roughly 4 T for  $x = 0.2, 0.3$  and  $0.4$ . Compounds with  $x > 0.5$  (i.e. compounds showing the spin glass state) exhibit the entropy shift to higher temperatures already for the lowest applied magnetic field of 2 T.

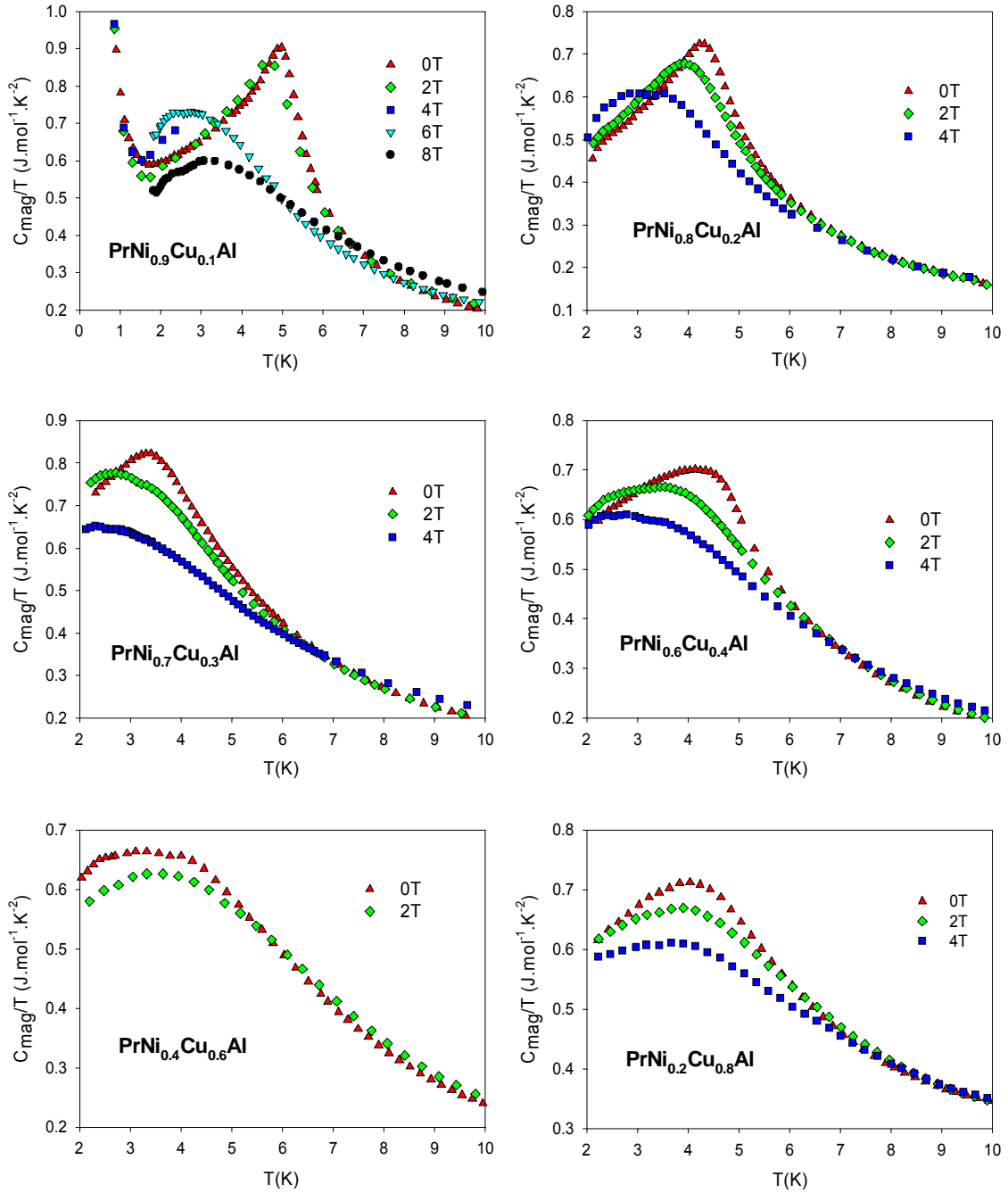


Fig. 5.27.:  $C_{mag}/T(T)$  dependencies under an applied magnetic field.

## 5.5. Powder neutron diffraction

Powder neutron diffraction was measured on  $\text{PrNi}_{0.2}\text{Cu}_{0.8}\text{Al}$ . In Fig. 5.28., there are shown the results of measurements performed in the temperature of 20 K, which is well above the transition temperature of  $\text{PrNi}_{0.2}\text{Cu}_{0.8}\text{Al}$ , and in the temperature of 1.3 K which is below the transition temperature.

When we compare the two patterns, there are visible hardly any differences between them. The only exception is a small broad peak which appears in the second pattern around the angle of 15 degrees (marked by the vertical arrow). The absence of any magnetic reflections below the ordering temperature shows on no existence of long range order in this compound which is in agreement with results from the previous sections. If we take a look on diffraction patterns measured previously on the  $\text{RNi}_{1-x}\text{Cu}_x\text{Al}$  ( $R = \text{Dy}, \text{Er}$ ) series [13, 32] (see section 3.1.), we can see that in both cases an enhanced intensity appears in the lowest angles (in comparison with paramagnetic state patterns) in compounds exhibiting the loss of long range order. This effect was a sign of ferromagnetic short range correlations manifesting by the increased intensity near the (0 0 0) reflection. By contrary, in our sample the intensity in the lowest angles only slightly differs between the two measured temperatures showing on no ferromagnetic correlations to be present. Additionally, the small bump around the angle of 15 degrees could be sign of a similar behavior to the one reported in the  $\text{ErNi}_{1-x}\text{Cu}_x\text{Al}$  series [1] where broadening of peaks occurs in the compounds exhibiting the loss of long range order, see Fig. 3.5. Our bump could correspond to the magnetic peak in  $\text{PrCuAl}$  pattern which is quite close to it, see inset Fig. 5.28., corroborating the possible antiferromagnetic correlations in  $\text{PrNi}_{0.2}\text{Cu}_{0.8}\text{Al}$ .

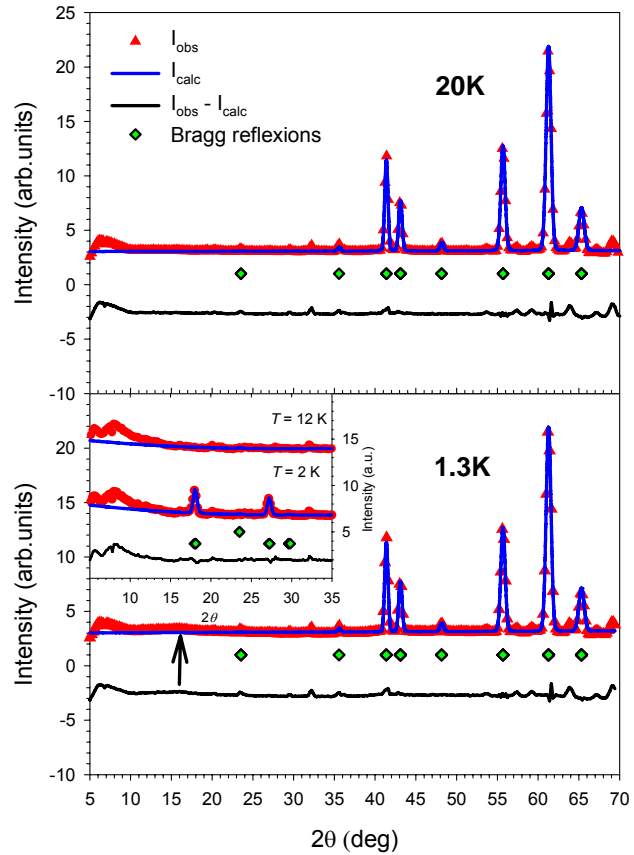


Fig. 5.28.: Powder neutron diffraction patterns of  $\text{PrNi}_{0.2}\text{Cu}_{0.8}\text{Al}$  measured in the temperatures of 20 and 1.3 K. The arrow points to a small bump around the angle of 15 degrees. The inset shows powder neutron diffraction pattern of  $\text{PrCuAl}$  [30].

## 6. Conclusions

We have studied structural and magnetic properties of the  $\text{PrNi}_{1-x}\text{Cu}_x\text{Al}$  series by means of X-ray diffraction, magnetization, specific heat and neutron diffraction. Measurements were in all cases performed on polycrystalline samples.

Structural results confirm expected behavior when the lattice parameters change monotonously with the parameter  $x$  in the range lying between the values of parental compounds  $\text{PrNiAl}$  and  $\text{PrCuAl}$ .

In the paramagnetic region all of the compounds show the typical Curie-Weiss dependence. Paramagnetic Curie temperatures are in all cases negative and effective moments are close to the  $\text{Pr}^{3+}$  free ion value which is also in conformity with  $\text{PrNiAl}$  and  $\text{PrCuAl}$ . The negative paramagnetic temperatures indicate prevailing antiferromagnetic interactions in the paramagnetic state.

The crystal field energy scheme, determined from the Schottky contribution to the specific heat, does not change significantly throughout the series. Quasi-doublet ground state (energy separation  $\approx 10$  K) is observed for all the measured samples.

Results on magnetic properties show on development of a long range magnetic order in  $\text{PrNi}_{1-x}\text{Cu}_x\text{Al}$  for  $x \leq 0.4$ . All these compounds order antiferromagnetically below  $T_N \approx 4$  K which is considerably lower than in case of  $\text{PrNiAl}$  and  $\text{PrCuAl}$ . The complexity of the magnetic order is manifested by appearance of another magnetic phase transition around the temperature of 2.1 K in  $\text{PrNi}_{0.9}\text{Cu}_{0.1}\text{Al}$ . The results of AC susceptibility measurements on the rest of the series ( $x \geq 0.5$ ) revealed a loss of long range magnetic order manifesting itself via the frequency dependent maxima of  $\chi_{AC}'$  vs.  $T$  dependencies. The loss of long range magnetic order is corroborated also by the results of magnetization and specific heat measurements. The neutron diffraction experiment on  $\text{PrNi}_{0.2}\text{Cu}_{0.8}\text{Al}$  confirms this feature. Additionally, it points to an antiferromagnetic type of short range correlations which differs from the  $\text{RNi}_{1-x}\text{Cu}_x\text{Al}$  ( $R = \text{Er}, \text{Dy}$ ) series where ferromagnetic short range correlations had been observed. Another difference compared to the Tb, Er and Dy based series comes out by wider concentration region of the spin glass behavior, alike to the recently published  $\text{NdNi}_{1-x}\text{Cu}_x\text{Al}$  series. It seems to be a general difference between the light and the heavy rare earth based  $\text{RNi}_{1-x}\text{Cu}_x\text{Al}$  compounds.

## References

- [1] J. Prchal: Ph.D. thesis, 2006 (UK MFF), Prague
- [2] P. Javorský, L. Havela, V. Sechovsky, H. Michor, K. Jurek, Magnetic behaviour of RCuAl compounds, *Journal of Alloys and Compounds*, Volume 264, Issues 1-2, 9 January 1998, Pages 38-42
- [3] P. Javorský, V. Sechovský, L. Havela, H. Michor, *Journal of Magnetism and Magnetic Materials*, Volumes 177-181, Part 2, January 1998, Pages 1052-1053
- [4] ILL07 proposal list
- [5] P. Javorský, P. Burllet, V. Sechovsky, R. R. Arons, E. Ressouche, G. Lapertot, Neutron diffraction study of magnetic ordering in RNiAl compounds, *Physica B: Condensed Matter*, 1997, Volumes 234-236, Pages 665-666
- [6] G. Ehlers, H. Maletta, Frustrated magnetic moments in RNiAl intermetallic compounds, *Physica B: Condensed Matter*, Volumes 234-236, 1997, Pages 667-669
- [7] M.A. Ruderman and C. Kittel, *Phys. Rev.* 96, 99 (1954)
- [8] P. Javorský, V. Sechovsky, R. R. Arons, P. Burllet, E. Ressouche, P. Svoboda, G. Lapertot, Neutron diffraction study of magnetic ordering in NdNiAl and PrNiAl, *Journal of Magnetism and Magnetic Materials*, Volume 164, Issues 1-2, 2 November 1996, Pages 183-186
- [9] G. Ehlers, D. Ahlert, W. Miekeley, H. Maletta, Change from antiferromagnetic to ferromagnetic order in the pseudo-ternary series TbNi<sub>1-x</sub>Cu<sub>x</sub>Al, *Physica B: Condensed Matter*, Volumes 234-236, 1997, Pages 670-672
- [10] P. Javorský, P. Burllet, E. Ressouche, V. Sechovsky, H. Michor, G. Lapertot, Magnetic structure study of ErCuAl and ErNiAl, *Physica B: Condensed Matter*, Volume 225, Issues 3-4, 1996, Pages 230-236
- [11] J. Prchal, P. Javorský, O. Isnard, V. Sechovsky, Neutron-diffraction study of the ErNi<sub>1-x</sub>Cu<sub>x</sub>Al series, *Physica B: Condensed Matter*, Volume 350, Issues 1-3, 2004, Pages E159-E161
- [12] P. Javorský, L. Havela, V. Sechovsky, H. Michor, K. Jurek, Magnetic behaviour of RCuAl compounds, *Journal of Alloys and Compounds*, Volume 264, Issues 1-2, 1998, Pages 38-42
- [13] J. Prchal, P. Javorský, B. Detlefs, S. Danis, O. Isnard, Magnetic structures in DyNi<sub>1-x</sub>Cu<sub>x</sub>Al pseudoternaries, *Journal of Magnetism and Magnetic Materials*, Volume 310, 2007, Pages e589-e591
- [14] J. Prchal, M. Mísek, P. Javorský, J. Vejpravova, ISIS experimental report

- [15] J. Prchal, E. Santava, D. Schmoranzer, Spin-glass behavior of  $RNi_{1-x}Cu_xAl$  compounds, *Physica B: Condensed Matter*, Volume 404, Issue 19, 2009, Pages 3056-8
- [16] J. Prchal, et al., *Intermetallics*, to be submitted
- [17] I.A.Campbell, *J. Phys. F: Metal Phys.*, 2, L47 (1972)
- [18] Ch.Kittel, *Úvod do fyziky pevných látek*, Academia, Praha, 1985
- [19] David R. Lide (ed), *CRC Handbook of Chemistry and Physics, 84th Edition*, online version, CRC Press, Boca Raton, Florida, 2003; Section 4, Properties of the Elements and Inorganic Compounds; Vapor Pressure of the Metallic Elements
- [20] J. Rodriguez-Carvajal, *Physica B* 192, 55 (1993)
- [21] M.T.Hutchings, *Solid state physics*, 16 (1964) 227
- [22] S. Blundell, *Magnetism in condensed matter*, Oxford University Press, 2001
- [23] K. Binder and A.P. Young, *Rev. Mod. Phys.* **58** (1986), pp. 801–976
- [24] L.Néel, *Annales de Géophysique*, 5 (1949) 99
- [25] E.P.Wohlfarth, *Physica B+C*, 86-88 (1977) 852
- [26] S. Shtrikman, E. P. Wohlfarth, The theory of the Vogel-Fulcher law of spin glasses, *Physics Letters A*, Volume 85, Issues 8-9, 1981, Pages 467-470
- [27] Ch. Kittel, *Úvod do fyziky pevných látek*, Academia, Prague, 1985. (2008)
- [28] V. F. Sears, *Neutron News*, 3 (1992) 26
- [29] C. Stassis, H. W. Deckman, .N. Harmon, J. P. Desclaux, A. J. Freeman, *Physical Review B*, 15 (1977) 369
- [30] P. Javorský, J. Kaštil, O. Isnard, Non-collinear antiferromagnetic structure in  $PrCuAl$ , in press to *J. Phys.: Conference Series*; ILL report
- [31] G.Ehlers, H.Maletta, *Zeitschrift für Physik B* 101, 317-327 (1996)
- [32] J. Prchal, P. Javorský, V. Sechovský, M. Dopita, O. Isnard, K. Jurek, *Journal of Magnetism and Magnetic Materials* 283, 34 (2004)
- [33] N.C.Tuan et al., *J. Appl. Phys.* 73 (1993) 5677
- [34] P Javorský, P Daniel, E Santava, J Prchal, Change of crystal field in the  $Er(Ni,Cu)Al$  system, *J. Magn. Magn. Mat.*, 316 (2007), e400-e402
- [35] D. X. Li, Y. Shiokawa, S. Nimori, Y. Haga, E. Yamamoto, T. D. Matsuda, Y. Onuki, Magnetic behavior in nonmagnetic atom disorder system  $Ce_2CuSi_3$ , *Physica B: Condensed Matter*, Volumes 329-333, Part 2, 2003, Pages 506-507
- [36] P. Javorský, H.Mutka, H.Nakotte, *Apl. Phys. A* 74, S658-S660 (2002)
- [37] N. W. Ashcroft, N. D. Mermin: *Solid State Physics*, Saunders College, Philadelphia 1976.
- [38] A.E.Dwight, M.H.Muller, R.A.Conner Jr., J.W.Downey, H.Knott, *Trans. Met. Soc. AIME* 242, 2075 (1968)